J|A|C|S

A R T I C L E S

Low-Spin Ferriheme Models of the Cytochromes: Correlation of Molecular Structure with EPR Spectral Type[†]

Liliya A. Yatsunyk, Michael D. Carducci, and F. Ann Walker*

Contribution from the Department of Chemistry, University of Arizona, Tucson, Arizona 85721-0041

Received May 28, 2003; E-mail: awalker@u.arizona.edu

Abstract: The preparation and characterization of the following bis-imidazole and bis-pyridine complexes of octamethyltetraphenylporphyrinatoiron(III), Fe(III)OMTPP, octaethyltetraphenylporphyrinatoiron(III), Fe-(III)OETPP, and tetra-β,β'-tetramethylenetetraphenylporphyrinatoiron(III), Fe(III)TC$_6$TPP, are reported: *paral*-[FeOMTPP(1-MeIm)$_2$]Cl, *perp*-[FeOMTPP(1-MeIm)$_2$]Cl, [FeOETPP(1-MeIm)$_2$]Cl, [FeTC$_6$TPP(1-MeIm)$_2$]Cl, [FeOMTPP(4-Me$_2$NPy)$_2$]Cl, and [FeOMTPP(2-MeHIm)$_2$]Cl. Crystal structure analysis shows that *paral*-[FeOMTPP(1-MeIm)$_2$]Cl has its axial ligands in close to parallel orientation (the actual dihedral angle between the planes of the imidazole ligands is 19.5°), while *perp*-[FeOMTPP(1-MeIm)$_2$]Cl has the axial imidazole ligand planes oriented at 90° to each other and 29° away from the closest N$_P$–Fe–N$_P$ axis. [FeOETPP-(1-MeIm)$_2$]Cl has its axial ligands close to perpendicular orientation (the actual dihedral angle between the planes of the imidazole ligands is 73.1°). In all three cases the porphyrin core adopts relatively purely saddled geometry. The [FeTC$_6$TPP(1-MeIm)$_2$]Cl complex is the most planar and has the highest contribution of a ruffled component in the overall saddled structure compared to all other complexes in this study. The estimated numerical contribution of saddled and ruffled components is 0.68:0.32, respectively. Axial ligand planes are perpendicular to each other and 15.3° away from the closest N$_P$–Fe–N$_P$ axis. The Fe–N$_P$ bond is the longest in the series of octaalkyltetraphenylporphyrinatoiron(III) complexes due to [FeTC$_6$TPP-(1-MeIm)$_2$]Cl having the least distorted porphyrin core. In addition to these three complexes, two crystalline forms each of [FeOMTPP(4-Me$_2$NPy)$_2$]Cl and [FeOMTPP(2-MeHIm)$_2$]Cl were obtained. In all four of these cases the axial planes are in nearly perpendicular planes in spite of quite different geometries of the porphyrin cores (from purely saddled to saddled with 30% ruffling). The EPR spectral type correlates with the geometry of the OMTPP, OETPP and TC$_6$TPP complexes. For the *paral*-[FeOMTPP(1-MeIm)$_2$]Cl, a rhombic signal with $g_1 = 1.54$, $g_2 = 2.51$, and $g_3 = 2.71$ is consistent with nearly parallel axial ligand orientation. For all other complexes of this study, "large g_{max}" signals are observed ($g_{max} = 3.61 - 3.27$), as are observed for nearly perpendicular ligand plane arrangement. On the basis of this and previous work, the change from "large g_{max}" to normal rhombic EPR signal occurs between axial ligand plane dihedral angles of 70° and 30°.

Introduction

Bis-histidine-coordinated heme centers are involved in electron transfer in a number of cytochrome-containing systems including complexes II, III, and IV of inner mitochondrial membranes. Complex III, also called the cytochrome bc_1 complex or ubiquinol:cytochrome c oxidoreductase, plays an important role in electron-transfer processes in mitochondria, chloroplasts, and in many aerobic and photosynthetic bacteria. It transfers electrons from ubiquinol to soluble cytochrome c; this process is coupled to translocation of two protons across the inner mitochondrial membrane. Several crystal structures of this complex have been reported[1–4] but they do not have high enough resolution to obtain the precise structure of the heme center with regard to the orientation of the axial ligands. It is believed that the arrangement of the axial ligands plays an important role in defining the spectroscopic properties, and possibly also the reduction potentials of these heme centers.

One of the first and most useful spectroscopic tools that provided much insight into the number, structure, properties, and roles of heme centers in the cytochrome bc_1 complex was EPR spectroscopy. The unusual EPR spectra for the cytochromes bc_1 were first reported by Orme-Johnson, Hansen, and Beinert[5] and later analyzed in detail by Salerno.[6] EPR data for the bc_1 complex show that both of the b hemes (as well as the c_1 heme)

(1) Xia, D.; Yu, C.-A.; Kim, H.; Xia, J.-Z.; Kachurin, A. M.; Zhang, L.; Yu, L.; Deisenhofer, J. *Science* **1997**, *277*, 60–66.
(2) Iwata, S.; Lee, J. W.; Okada, K.; Lee, J. K.; Iwata, M.; Rasmussen, B.; Link, T. A.; Ramaswamy, S.; Jap, B. K. *Science* **1998**, *281*, 64–71.
(3) Hunte, C.; Koepke, J.; Lange, C.; Rossmanith, T.; Michel, H. *Structure* **2000**, *8*, 669–684.
(4) Zhang, Zh.; Huang, L.; Shulmeister, V. M.; Chi, Y.-I.; Kim, K. K.; Hung, L.-W.; Crofts, A. R.; Berry, E. A.; Kim, S.-H. *Nature* **1998**, *392*, 677–684.

exhibit single feature EPR signals known as the "large g_{max}" [7] or "HALS" (highly anisotropic low-spin)[8,9] type. These signals are observed at temperatures below about 10 K, and all have the only resolved feature, the g_{max} signal, with the g-value $\geq$ 3.2 and with the other two g-values undetectable. For the cytochrome bc_1 complex of mitochondria and the related cytochrome b_6f complex of chloroplasts, these signals "relax" to normal rhombic EPR signals when the cytochrome b protein is extracted from the mitochondrial membrane and the other proteins of the complex.[10,11] At the highest resolution obtained thus far (2.2 Å),[12] the cytochrome bc_1 structure has been modeled with the two b heme centers having axial histidine imidazole plane dihedral angles of 84° and 38°. On the basis of redox titration, the former heme center, called b_L, was assigned the EPR signal with g_{max} = 3.75−3.78 and the latter one, called b_H, the EPR signal with g_{max} = 3.41−3.44.[5,6] Typical reduction potentials for the b_H and b_L centers of bovine heart complex III are 105 and −5 mV, respectively.[13]

Model systems have been great aids in correlating the structure of heme centers with their spectroscopic properties. In the early 1980s it was shown that the "large g_{max}" signal can be created for model ferrihemes by binding bulky imidazoles (2-methylimidazole, 1,2-dimethylimidazole, etc.) or some pyridines (3,4-dimethylpyridine, pyridine itself, etc.) to iron(III) tetraphenylporphyrin (TPPFe(III))[14] or ProtoIXFe(III).[8,9] Later, Walker, Scheidt, and their co-workers showed that the "large g_{max}" signal occurs for ferriheme complexes with $(d_{xy})^2(d_{xz},d_{yz})^3$ electronic ground states when the axial ligands are in perpendicular planes,[7,15] and hence established the first correlation of structure with EPR spectral type: "large g_{max}" → axial ligands in perpendicular planes; normal rhombic → axial ligands in parallel planes. "Large g_{max}" signals are observed for ferriheme complexes in which the splitting between the d_{xz} and d_{yz} orbitals is very small (less than the value of the spin−orbit coupling constant, λ, or $\ll$400 cm^{-1}),[7,19] i.e., the case where axial ligands are in perpendicular planes or where ligands without planes are used (e.g., CN$^-$, phosphines or NH$_3$),[16−18] whereas normal rhombic EPR signals are observed when the splitting between these two orbitals is larger, on the order of 2−3 times the spin−orbit coupling constant, λ, or 600−1000 cm^{-1},[7,19] i.e., when planar axial ligands coordinated to iron are oriented in parallel planes. It is interesting to note that the smaller of the dihedral angles of the b hemes of the cytochrome bc_1 complex (38°) does not appear to be consistent with the fact that a "large g_{max}" signal is observed for both b hemes.

Previous systems investigated as models of these bis-histidine-coordinated cytochromes b have all utilized synthetic hemes such as octaethylporphyrinatoiron(III)/(II) (OEPFe) or tetraphenylporphyrinatoiron(III)/(II) (TPPFe), or other tetraarylporphyrin-type systems such as tetramesitylporphyrinatoiron(III)/(II) (TMPFe).[20,24,25] These systems often adopt nonplanar porphyrin ring conformations due to steric interaction between the peripheral substituents or between the porphyrin and the axial ligands. In general, there are four major types of nonplanar distortion: saddled, ruffled, domed, and waved,[21] with saddled and ruffled distortions being the most commonly observed in the model systems. In the saddled conformation, adjacent pyrrole rings are tilted up and down with respect to the porphyrin mean plane and the *meso*-carbons are in the plane, while in the ruffled conformation the adjacent pyrrole rings are twisted clockwise and counterclockwise, bringing the *meso*-carbons above and below the porphyrin mean plane. Both ruffling and saddling result in the formation of two mutually perpendicular cavities, one above and one below the macrocycle plane;[22,23] these cavities are thus capable of orienting the planar aromatic axial ligands perpendicular to each other. In the case of the saddled conformation, the axial ligands are expected to be near the porphyrin nitrogens or nearly eclipsed with the N$_P$−Fe−N$_P$ vectors. In the ruffled conformation the axial ligands are oriented above the porphyrin *meso*-carbons or, in other words, form an approximately 45° angle with the closest N$_P$−Fe−N$_P$ vector. It has been found that for low-spin (LS) Fe(III) porphyrinates, all of the TPP- and TMP-derived systems studied previously adopt ruffled conformations when the axial ligands are in perpendicular planes lying at ∼45° to the N$_P$−Fe−N$_P$ vectors, i.e., when the axial ligands are hindered imidazoles (2-MeHIm, 1,2-Me$_2$Im) or pyridines.[20,24−26] However, for the Fe(II) analogues of these TPP/TMP complexes, no structure of a bis-hindered imidazole complex has been reported, and all structures of bis-pyridine complexes have the axial ligands in parallel planes lying at about 45° to one of the N$_P$−Fe−N$_P$ vectors, with the conformation of the porphyrin ring being planar.[27] Hence, it appears that pyridine ligands are capable of binding to iron(II) porphyrinates without ruffling of the porphyrin ring. To summarize, then, for *meso*-only substituted Fe(III) (LS d^5) porphyrinates with bulky axial ligands and/or *meso*-substituents, the preferred geometry is with axial ligands in perpendicular planes and a ruffled porphyrin ring, while for Fe(II) (LS d^6) porphyrinates, the preferred geometry of all bis-ligand complexes for which structures have been reported is with axial ligands in parallel planes and a planar porphyrin ring. The fact that hindered (2-substituted) imidazoles cannot bind to Fe porphyrinates of either oxidation state unless they are placed in

(5) Orme-Johnson, N. R.; Hansen, R. E.; Beinert, H. *Biochem. Biophys. Res. Commun.* **1971**, *45*, 871−878.
(6) Salerno, J. C. *J. Biol. Chem.* **1984**, *259*, 2331−2336.
(7) Walker, F. A.; Huynh, B. H.; Scheidt, W. R.; Osvath, S. R. *J. Am. Chem. Soc.* **1986**, *108*, 5288−5297.
(8) Migita, C. T.; Iwaizumi, M. *J. Am. Chem. Soc.* **1981**, *103*, 4378.
(9) Carter, K. R.; T'sai, A.-L.; Palmer, G. *FEBS Lett.* **1981**, *132*, 243−246.
(10) T'sai, A.-L.; Palmer, G. *Biochim. Biophys. Acta* **1982**, *681*, 484−495.
(11) . Salerno, J. C.; McGill, J. W.; Gerstle, G. C. *FEBS Lett.* **1983**, *162*, 257−261.
(12) Iwata, S. Personal communication.
(13) Von Jagow, G.; Engel, W. D. *Angew Chem., Int. Ed. Engl.* **1980**, *19*, 659−675.
(14) Walker, F. A.; Reis, D.; Balke, V. L. *J. Am. Chem. Soc.* **1984**, *106*, 6888−6898.
(15) Scheidt, W. R.; Kirner, J. F.; Hoard, J. L.; Reed, Ch. A. *J. Am. Chem. Soc.* **1987**, *109*, 1963−1968.
(16) Innis D.; Soltis, S. M.; Strouse, C. E. *J. Am. Chem. Soc.* **1988**, *110*, 5644−5650.
(17) Watson, C. T.; Walker, F. A., unpublished data.
(18) Ikeue, T.; Ohgo, Y.; Saitoh, T.; Yamaguchi, T.; Nakamura, M. *Inorg. Chem.* **2001**, *40*, 3423−3434.
(19) Walker, F. A. *Coord. Chem. Rev.* **1999**, *185−186*, 471−534.

(20) Munro, O. Q.; Serth-Guzzo, J. A.; Turowska-Tyrk, I.; Mohanrao, K.; Shokhireva, T. Kh.; Walker, F. A.; Debrunner, P. G.; Scheidt, W. R. *J. Am. Chem. Soc.* **1999**, *121*, 11144−11155.
(21) http://www.chem.ucdavis.edu/groups/smith/chime/structs/ruf_structs.html.
(22) Walker, F. A.; Simonis, U. *J. Am. Chem. Soc.* **1991**, *113*, 8652−8657. Walker, F. A.; Simonis, U. *J. Am. Chem. Soc.* **1992**, *114*, 1929.
(23) Sparks, L. D.; Medforth, C. J.; Park, M. S.; Chamberlain, J. R.; Ondrias, M. R.; Senge, M. O.; Smith, K. M.; Shelnutt, J. A. *J. Am. Chem. Soc.* **1993**, *115*, 581−592.
(24) Safo, M. K.; Gupta, G. P.; Walker, F. A.; Scheidt, W. R.; *J. Am. Chem. Soc.* **1991**, *113*, 5497−5510.
(25) Safo, M. K.; Gupta, G. P.; Walker, F. A.; Watson, C. T.; Simonis, U.; Scheidt, W. R. *J. Am. Chem. Soc.* **1992**, *114*, 7066−7075.
(26) Munro, O. Q.; Marques, H. M.; Debrunner, P. G.; Mohanrao, K.; Scheidt, W. R. *J. Am. Chem. Soc.* **1995**, *117*, 935−954.
(27) Safo, M. K.; Nesset, M. J. M.; Walker, F. A.; Debrunner, P. G.; Scheidt, W. R. *J. Am. Chem. Soc.* **1997**, *119*, 9438−9448.

perpendicular planes (because of the bulky 2-substituent), along with the fact that bis-hindered imidazole complexes of Fe(II) porphyrinates are very unstable and can only be formed and studied at extremely low temperatures,[28,29] suggests that Fe(II) porphyrinates having a ruffled core are thermodynamically unstable. DFT calculations of Mössbauer parameters at 4.2 K support a perpendicular ligand orientation with ruffled porphyrin core for the bis-2-methylimidazole complex of TMPFe(II),[30] which only forms at very low temperatures.[29]

Cytochromes *b* are redox proteins, and thus both oxidation states must be structurally stable, with little reorganizational energy involved in the redox process. In this regard, it is unreasonable to think that the ligands can change from perpendicular (Fe(III)) to parallel (Fe(II)) upon redox. Hence, to model the bis-histidine-coordinated heme centers of the bc_1 complex, in which it appears that at least one of the hemes has the histidine ligands in perpendicular planes,[1–4] TPP/TMP-derived iron porphyrinates do not appear to reproduce the structures and properties of both the Fe(III) and Fe(II) oxidation states. Thus model hemes must be found that will support perpendicular ligand planes for both oxidation states of iron. Therefore, we have turned to an investigation of the octaalkyltetraphenylporphyrin complexes of iron as possible model hemes that could support perpendicular ligand orientations not only for Fe(III) but also for Fe(II). Since all of these complexes adopt predominantly saddled conformations, it was expected that the axial ligand planes would be perpendicular and oriented above or nearly above the porphyrin nitrogens.

Along with the lack of structural data on Fe(II) porphyrinates with perpendicular axial ligands and a ruffled porphyrinate core, redox data strongly indicate that complexes with bulky ligands that would have to bind in a perpendicular orientation over the *meso* positions (i.e., just the right situation to encourage ruffling) have very negative reduction potentials compared to those having nonbulky ligands that can bind in parallel planes and maintain a planar porphyrin ring (−212 mV as compared to −130 mV vs SCE for 2-MeHIm and 1-MeIm, respectively, for TMPFe).[31] The more negative reduction potential means that the Fe(III) state is strongly stabilized over the Fe(II) state when hindered imidazoles are bound to the metal. The derived binding constants support this (log β_2^{III} = 7.4 and 7.9, respectively, while log β_2^{II} = 5.5 and 7.3, respectively, for TMPFe complexes of 2-MeHIm and 1-MeIm).[31]

In our earlier publication on bis-axial ligand complexes of octaethyltetraphenylporphyrinatoiron(III), Fe(III)OETPP,[32] we found that the bis-2-MeHIm complex had perpendicular axial ligand planes, offset from the N_P–Fe–N_P axes by 14°, a very small angle as compared to TPP and TMP complexes of Fe-(III) with hindered imidazoles,[15,20] while the bis-4-Me₂NPy complex had a 70° dihedral angle between axial ligand planes, and the smallest angle yet observed for bis-pyridine complexes between the ligand plane and the N_P–Fe–N_P axis of 9°, yet

both of these complexes had "large g_{max}" EPR signals.[32] Thus, it is clear that an axial ligand plane dihedral angle of 70° is sufficiently large to yield a "large g_{max}" EPR signal. This is a very important finding with respect to the membrane-bound cytochromes *b*,[1–4] for it indicates that the observed "large g_{max}" EPR signals[6] could be expected if the dihedral angles between histidine ligand planes were as small as 70°. Determining how much smaller than 70° this dihedral angle could be and yet give rise to a "large g_{max}" EPR signal was one of the goals of this work.

In this paper we describe the crystal structures and EPR spectra of eight crystalline forms of octaalkyltetraphenylporphyrinatoiron(III) with different axial ligands. All of the iron porphyrinate molecules in this study adopt predominantly saddled conformations, and we find that this class of synthetic porphyrinates is exceptionally rich in stabilizing a variety of axial ligand orientations, dihedral angles, and porphyrin core conformations. The overall goal of this project is to determine the limits on axial ligand plane dihedral angle for each type of EPR and Mössbauer signal and to see if there is any correlation between *g*-values or Mössbauer spectral parameters observed and ligand plane dihedral angle. This is being done by determining the molecular structures of a series of mainly saddled Fe(III) and Fe(II) octaalkyltetraphenylporphyrinate complexes, in the hope of finding nonruffled porphyrinate cores that will stabilize the Fe(II) state with perpendicular axial ligand planes. A related goal of this project is to measure the reduction potentials of the complexes that are characterized structurally and spectroscopically, to correlate the geometry of the active site at the heme center in models and proteins with the reduction potential of the heme, as well as with the EPR spectrum of the Fe(III) state of the center and the Mössbauer spectra of both oxidation states. The Mössbauer spectra of four of these LS ferriheme complexes are presented elsewhere.[33]

Experimental Section

Synthesis of (OMTPP)FeCl. Octamethyltetraphenylporphyrin (H₂-OMTPP) was prepared by first synthesizing 3,4-dimethylpyrrole.[34] Next, the porphyrinogen was synthesized by reaction of the pyrrole with benzaldehyde and oxidized with 2,3-dichloro-5,6-dicyano-1,4-benzoquinone (DDQ), according to the literature procedure[35] except that both steps (condensation and oxidation) were done in one reaction flask. The product was purified by column chromatography (3 × 30 cm³ Alumina, Brockman grade III). Elution first with 1:1 CH₂Cl₂:C₆H₆, next with CH₂Cl₂, and finally with 2% methanol in CH₂Cl₂ yielded the desired porphyrin, which eluted as a very narrow dark green band (probably in the form of H₄OMTPP²⁺) in the final step. Solvent was removed under reduced pressure, and the resulting material was redissolved in a small quantity of CH₂Cl₂ and recrystallized from 0.2% KOH in ethanol. Iron was inserted using anhydrous iron(II) chloride (Aldrich) in DMF[36] with subsequent recrystallization of the product from CH₂Cl₂/ether solvent mixtures. A quantitative yield of (OMTPP)-FeCl crystals was obtained.

Synthesis of (OETPP)FeCl. Octaethyltetraphenylporphyrin (H₂-OETPP) was prepared by first synthesizing 3,4-diethylpyrrole.[34–36] The

(28) Polam, J. R.; Wright, J. L.; Christensen, K. A.; Walker, F. A.; Flint, H.; Winkler, H.; Grodzicki, M.; Trautwein, A. X. *J. Am. Chem. Soc.* **1996**, *118*, 5272–5276.
(29) Polam, J. R.; Shokhireva, T. Kh.; Raffii, K.; Simonis, U.; Walker, F. A. *Inorg. Chim. Acta* **1997**, *263/1–2*, 109–117.
(30) Grodzicki, M.; Flint, H.; Winkler, H.; Walker, F. A.; Trautwein, A. X. *J. Phys. Chem. A* **1997**, *101*, 4202–4207.
(31) Nesset, M. J. M.; Shokhirev, N. V.; Enemark, P. D.; Jacobson, S. E.; Walker, F. A. *Inorg. Chem.* **1996**, *35*, 5188–5200.
(32) Ogura, H.; Yatsunyk, L.; Medforth, C. J.; Smith, K. M.; Barkigia, K. M.; Renner, M. W.; Melamed, D.; Walker, F. A. *J. Am. Chem. Soc.* **2001**, *123*, 6564–6578.

(33) Teschner, T.; Yatsunyk, L.; Schünemann, V.; Trautwein, A. X.; Walker, F. A. Manuscript in preparation.
(34) Cheng, D. O.; Bowman, T. L.; LeGoff, E. *Tetrahedron Lett.* **1976**, *13*, 1145–1147.
(35) Barkigia, K. M.; Berber, M. D.; Fajer, J.; Medforth, C. J.; Renner, M. W.; Smith, K. M. *J. Am. Chem. Soc.* **1990**, *112*, 8851–8857.
(36) Sparks, L. D.; Medforth, C. J.; Park, M.-S.; Chamberlain, J. R.; Ondrias, M. R.; Senge, M. O.; Smith, K. M.; Shelnutt, J. A. *J. Am. Chem. Soc.* **1993**, *115*, 581–592.

overall yield was 35% starting from the propionaldehyde. The porphyrinogen and porphyrin were then prepared as reported earlier[35] without the modification used for H$_2$OMTPP. Namely, the porphyrinogen was synthesized first, solvent was removed under reduced pressure, and the residue was washed with methanol, yielding a white precipitate which was filtered, redissolved in a small amount of CH$_2$Cl$_2$, and recrystallized from methanol again, yielding 48% of the pure porphyrinogen. It was oxidized with 4 equiv of DDQ, and the crude product was applied to a column of alumina (Brockman grade III, 2.5 × 15 cm^3 column) eluted first with CH$_2$Cl$_2$, next 2% methanol in CH$_2$Cl$_2$ and finally 2:1 CH$_2$Cl$_2$: methanol) and recrystallized from 0.2% KOH in ethanol. The resulting crystals were dried in a vacuum oven for 4 h at 70 °C. Yield 67%. Iron insertion was carried out as described above. An excellent method of purification of (OETPP)FeCl was discovered. After removal of the solvent, the dry residue was washed with pentane, yielding, after filtration, a dark brown powder of very pure (OETPP)FeCl. It was washed repeatedly with cold pentane and dried in the vacuum oven for 4 h at 70 °C.

Synthesis of (TC$_6$TPP)FeCl. (TC$_6$TPP)FeCl was synthesized according to literature procedures[37,38] with some modifications. First ethyl 3,4-butanopyrrole-2-carboxylate was synthesized using the procedure of Barton and Zard[39,40] from 1-nitrocylohexane and ethyl isocyanoacetate in the presence of guanidine base.[41,42] Hydrolysis and decarboxylation of ethyl 3,4-tetramethylenepyrrole-2-carboxylate with sodium hydroxide in refluxing ethylene glycol afforded 3,4-tetramethylenepyrrole in 32% yield (from 1-nitrocyclohexane).[39] Next, the porphyrinogen was prepared and oxidized with DDQ, according to the literature procedure[35] with the modification used for the H$_2$OMTPP synthesis. The solvent was evaporated to dryness, and the residue was taken up in CH$_2$Cl$_2$. The free-base porphyrin solution was applied to a column of alumina (3 × 30 cm^2, alumina Brockman Grade III, packed by the wet method with 1:1 CH$_2$Cl$_2$/C$_6$H$_6$ mixture) and eluted with 1:1 C$_6$H$_6$:CH$_2$Cl$_2$, then pure CH$_2$Cl$_2$, and finally 2% methanol in CH$_2$Cl$_2$. The desired porphyrin eluted as a narrow dark brown-green band with 2% methanol in CH$_2$Cl$_2$. Solvent was removed and the resulting material was dissolved in a small amount of hot CH$_2$Cl$_2$ and recrystallized from hot 0.2% KOH in ethanol. By cooling slowly and letting the solution stand at 5 °C, large crystals formed. The product was collected by filtration and dried in a vacuum oven for 4 h at 70 °C to afford 53 mg of blue needlelike crystals (21% yield). Fe insertion was done as described above. Large dark blue crystals suitable for X-ray structure determination were formed in 63% yield (from the porphyrin) after recrystallization from the CH$_2$Cl$_2$/ether. The optical spectrum of (TC$_6$TPP)FeCl shows a split Soret band: 397.3 nm (1.054), and 427.7 nm (0.967) and several poorly resolved bands in the 500–650 nm region of the spectrum, namely, 530.2 nm (0.177), 572.0 nm (0.135), and 707.5 nm (0.070). ^{1}H NMR (CD$_2$Cl$_2$, 600 MHz, 298 K, referenced to residual solvent peak at 5.32 ppm): δ ppm, 55.20 and 53.55 (s, 8H each, CH$_2$-(α)), 13.25 and 12.84 (s, 4H each, Ph-*m*), 9.40 and 6.85 (br, 4H each, Ph-*o*), 7.56 (s, 4H, Ph-*p*), 7.04 and 5.61 (s, 8H each, CH$_2(\beta)$).

1-Methylimidazole (1-MeIm), 4-(dimethylamino)pyridine (4-Me$_2$NPy), and 2-methylimidazole (2-MeHIm) complexes of (OMTPP)FeCl, (OETPP)FeCl, and (TC$_6$TPP)FeCl were obtained by simply placing 3–6 equiv of the chosen axial ligand in a methylene chloride solution of the chosen porphyrinatoiron(III) chloride. Crystals were grown by liquid diffusion methods. In most cases two solvent systems were used: (1) methylene chloride and dodecane; (2) chloroform and

cyclohexane. Usually deuturated methylene chloride and chloroform were used due to their high purity and dryness. Other solvent systems were tried as well, but these two were used most frequently and successfully. EPR spectra were recorded on a Bruker ESP-300E EPR spectrometer (operating at 9.4 GHz) equipped with Oxford Instruments ESR 900 continuous flow helium cryostat. Spectra were obtained for crystalline samples at 4 K. Microwave frequencies were measured using a Systron-Donner frequency counter. Typical values for microwave power, modulation frequency, and modulation amplitude were 0.2 mW, 100 kHz, and 1 G, respectively.

Computational Methods. Ab inito DFT calculations with the unrestricted hybrid method B3LYP and relatively small 3-21G basis set were applied to study the optimal ligand orientation in the nonplanar porphyrin molecules. The calculations were carried out using the commercial program package Gaussian 98,[43] and models were generated using Spartan 5.1. All coordinates were taken from the crystal structures of [FeOETPP(4-Me$_2$NPy)$_2$]Cl[32] and [FeOMTPP(4-Me$_2$NPy)$_2$]Cl (structures A and B) discussed below. No geometry optimization was performed; single-point calculations were done in all cases. First, porphyrin core models for all three complexes were generated from the crystal structures by removing axial 4-Me$_2$NPy ligands and substituting peripheral groups, Me, Et, and Ph with H. In each case we obtained the following porphyrin core: FeN$_4$C$_{20}$H$_{12}$. Then two pyridine ligands were added to each model (first they were oriented in the same way as in the crystal structures (see Table 2 below) and then one of them was constrained to be at 0° to the N$_P$−Fe−N$_P$ vector) and the single-point energies were calculated again. For the B:[FeOMTPP(4-Me$_2$NPy)$_2$]Cl complex, structures with different ligand orientation were generated. The angle between two ligand planes was fixed to 88.5°, and both ligands were rotated simultaneously in steps of 15°.

Structure Determination. General. Crystals of each complex were mounted on glass fibers in random orientation and examined on a Bruker SMART 1000 CCD detector X-ray diffractometer at 100(2) K for *paral*- and *perp*-[FeOMTPP(1-MeIm)$_2$]Cl, at 170(2) K for [FeOETPP(1-MeIm)$_2$]Cl, [FeTC$_6$TPP(1-MeIm)$_2$]Cl, [FeOMTPP(2-MeIm)$_2$]Cl (molecule C and D), and [FeOMTPP(4-Me$_2$NPy)$_2$]Cl (molecule B), and at 200(2) K for [FeOMTPP(4-Me$_2$NPy)$_2$]Cl, molecule A. All measurements utilized graphite-monochromated Mo Kα radiation (λ = 0.71073 Å) with a power setting of 50 kV, 40 mA. Final cell constants and complete details of the intensity collection and least squares refinement parameters for all complexes are summarized in Table 1 and in the Supporting Information.

In most cases, a total of 3736 frames at 1 detector setting covering 0 < 2θ < 60° were collected, having an omega scan width of 0.2° and an exposure time of 20 s per frame. In the case of A:[FeOMTPP(4-Me$_2$NPy)$_2$]Cl, [FeOETPP(1-MeIm)$_2$]Cl, and [FeOMTPP(2-MeHIm)$_2$]Cl (C and D), the exposure time was 10, 10, 60, and 60 s, respectively. The frames were integrated using the Bruker SAINT software package's narrow frame algorithm.[44] Initial cell constants and an orientation matrix for integration were determined from reflections obtained in three orthogonal 5° wedges of reciprocal space.

All structures were solved using SHELXS in the Bruker SHELXTL (Version 6.0) software package.[45] Refinements were performed using SHELXL, and illustrations were made using XP.[45] Solution was

(37) Medforth, C. J.; Senge, M. O.; Smith, K. M.; Sparks, L. D.; Shelnutt, J. A. *J. Am. Chem. Soc.* **1992**, *114*, 9859−9869.

(38) Medforth, C. J.; Berber, M. D.; Smith, K. M. *Tetrahedron Lett.* **1990**, *31* (26), 3719−33722.

(39) Barton, D. H. R.; Kervagoret, J.; Zard, S. Z. *Tetrahedron* **1990**, *26* (21), 7587−7598.

(40) Chen, Sh.; Lash, T. D. *J. Heterocycl. Chem.* **1997**, *34* (1), 273−278.

(41) Barton, D. H. R.; Elliot, J. D.; Gero, S. D. *J. Chem. Soc., Perkin Trans. I* **1982**, 2085−2090.

(42) Barton, D. H. R.; Elliot, J. D.; Gero, S. D. *J. Chem. Soc., Chem. Commun.* **1981**, 1136−1137.

(43) Gaussian 98, Revision A.7, Frisch, M. J.; Trucks, G. W.; Schlegel, H. B.; Scuseria, G. E.; Robb, M. A.; Cheeseman, J. R.; Zakrzewski, V. G.; Montgomery, Jr., J. A.; Stratmann, R. E.; Burant, J. C.; Dapprich, S.; Millam, J. M.; Daniels, A. D.; Kudin, K. N.; Strain, M. C.; Farkas, O.; Tomasi, J.; Barone, V.; Cossi, M.; Cammi, R.; Mennucci, B.; Pomelli, C.; Adamo, C.; Clifford, S.; Ochterski, J.; Petersson, G. A.; Ayala, P. Y.; Cui, Q.; Morokuma, K.; Malick, D. K.; Rabuck, A. D.; Raghavachari, K.; Foresman, J. B.; Cioslowski, J.; Ortiz, J. V.; Baboul, A. G.; Stefanov, B. B.; Liu, G.; Liashenko, A.; Piskorz, P.; Komaromi, I.; Gomperts, R.; Martin, R. L.; Fox, D. J.; Keith, D.; Al-Laham, M. A.; Peng, C. Y.; Nanayakkara, A.; Gonzalez, C.; Challacombe, M.; Gill, P. M. W.; Johnson, B.; Chen, W.; Wong, M. W.; Andres, J. L.; Gonzalez, C.; Head-Gordon, M.; Replogle, E. S.; Pople, J. A. Gaussian, Inc., Pittsburgh, PA, 1998.

(44) Bruker (2002) SAINT Reference Manual Version 6.0, Bruker AXS Inc., Madison, WI.

Table 1. Summary of Crystal Data and Intensity Collection Parameters

molecule	*paral*-[FeOMTPP(1-MeIm)$_2$]Cl·CD$_2$Cl$_2$	*perp*-[FeOMTPP(1-MeIm)$_2$]Cl·2.43CDCl$_3$	[FeOETPP(1-MeIm)$_2$]Cl·2CDCl$_3$·C$_6$H$_{12}$	[FeTC$_6$TPP(1-MeIm)$_2$]Cl·2CD$_2$Cl$_2$
emp form.	C$_{61}$H$_{58}$Cl$_3$FeN$_8$	C$_{62.43}$H$_{58.43}$Cl$_{8.3}$FeN$_8$	C$_{76}$H$_{86}$Cl$_7$FeN$_8$	C$_{70}$H$_{68}$Cl$_5$FeN$_8$
form. wt	1065.35	1270.89	1415.53	1244.34
temp, K	100(2)	100(2)	170(2)	170(2)
crystal system	monoclinic	cubic	monoclinic	tetragonal
space group	*Pc*	*I*-43*d*	*P*2$_1$	*I*4$_1$/*a*
a, Å	13.8856(10)	26.153(2)	12.860(2)	19.8263(17)
b, Å	10.1279(7)	26.153(2)	22.101(3)	19.8263(17)
c, Å	18.5327(13)	26.153(2)	13.791(2)	15.230(3)
α, β, γ, deg	90, 95.925(2), 90	90, 90, 90	90, 107.936(2), 90	90, 90, 90
volume, Å^3	2592.4(3)	17887(3)	3729.2(8)	5986.8(13)
Z	2	12	2	4
density (calc), g/cm^3	1.365	1.416	1.261	1.381
abs coeff., mm^{-1}	0.495	0.673	0.500	0.526
F(000)	1114	7874	1486	2580
crystal dimension, mm	0.46 × 0.25 × 0.06	0.49 × 0.48 × 0.37	0.49 × 0.33 × 0.20	0.26 × 0.20 × 0.12
θ limits	2.01 to 33.26	1.91 to 24.93	1.55 to 27.55	1.69 to 25.07
limiting indices	−21 ≤ *h* ≤ 21, −15 ≤ *k* ≤ 15, −28 ≤ *l* ≤ 28	−30 ≤ h ≤ 30, −30 ≤ *k* ≤ 30, −30 ≤ *l* ≤ 30	−16 ≤ *h* ≤ 16, −28 ≤ *k* ≤ 28, −17 ≤ *l* ≤ 17	−23 ≤ *h* ≤ 23, −23 ≤ *k* ≤ 23, −18 ≤ *l* ≤ 18
reflcns utilized	48078	93819	46562	27945
indep reflcns	18847 [R_{int} = 0.0367, R_σ = 0.059]	2578 [R_{int} = 0.0725, R_σ = 0.022]	17070 [R_{int} = 0.0446, R_σ = 0.063]	2647 [R(int) = 0.1287, R_σ = 0.090]
redundancy	2.55	36.4	2.73	10.6
reflcns with *I* > 2σ(*I*)	15443 (81.9%)	2544 (98.7%)	13710 (80.3%)	1389 (52.5%)
completeness, %	96.6	99.1	99.6	99.7
max and min. transmission	0.9709, 0.8042	0.7889, 0.7340	0.9066, 0.7918	0.999, 0.808
data/restraints/params	18847/5/683	2578/106/182	17070/49/829	2647/201/253
GoF on *F*^{2}	1.039	1.281	1.014	0.924
final *R* indices [*I* > 2σ(*I*)]	R_1 = 0.0481, wR$_2$ = 0.1109	R_1 = 0.0926, wR$_2$ = 0.2256	R_1 = 0.0563, wR$_2$ = 0.1338	R1 = 0.0565, wR$_2$ = 0.1458
R indices (all data)	R_1 = 0.0666, wR$_2$ = 0.1229	R_1 = 0.0935, wR$_2$ = 0.2261	R_1 = 0.0754, wR$_2$ = 0.1445	R_1 = 0.1219, wR$_2$ = 0.1731
largest diff. peak and hole, e/Å^3	0.764 and −0.731	0.250 and −0.204	0.676 and −0.410	0.488 and −0.474
RMS diff density, e/Å^3	0.081	0.054	0.071	0.062

molecule	A: [FeOMTPP(4-Me$_2$NPy)$_2$]Cl·4CD$_2$Cl$_2$	B: [FeOMTPP(4-Me$_2$NPy)$_2$]Cl·4CDCl$_3$	C: [FeOMTPP(2-MeHIm)$_2$]Cl·2CDCl$_3$	D: [FeOMTPP(2-MeHIm)$_2$]Cl·3CD$_2$Cl$_2$
emp form.	C$_{70}$H$_{72}$Cl FeN$_8$	C$_{70}$H$_{68}$Cl$_{13}$FeN$_8$	C$_{68}$H$_{70}$Cl$_7$FeN$_8$	C$_{63}$H$_{62}$Cl$_7$FeN$_8$
form. wt	1400.26	1538.02	1303.32	1235.21
temp, K	200(2)	170(2) K	170(2)	170(2)
crystal system	monoclinic	monoclinic	monoclinic	triclinic
space group	*C*2/*c*	*P*2$_1$/*c*	*P*2$_1$/*c*	*P*1̄
a, Å	21.766(5)	15.9507(13)	14.0780(14)	13.800(6)
b, Å	22.069(5)	23.2709(19)	26.710(3)	15.151(7)
c, Å	17.816(4)	19.5217(16)	17.2488(18)	16.566(8)
α, β, γ, deg	90, 127.096(3), 90	90, 94.396(2), 90	90, 96.765(2), 90	66.513(14), 71.841(13), 88.719(12)
volume, Å^3	6826(3)	7224.9(10)	6440.8(11)	2998(2)
Z	4	4	4	2
density (calc), g/cm^3	1.363	1.414	1.344	1.368
abs coeff., mm^{-1}	0.621	0.737	0.573	0.611
F(000)	2908	3164	2716	1282
crystal dimension, mm	0.55 × 0.40 × 0.28	0.55 × 0.25 × 0.25	0.28 × 0.06 × 0.02	0.20 × 0.08 × 0.08
θ limits, deg	1.85 to 27.70°	1.55 to 27.80	1.41 to 25.77	1.42 to 20.80
limiting indices	−27 ≤ *h* ≤ 26, −28 ≤ *k* ≤ 28, −23 ≤ *l* ≤ 22	−20 ≤ *h* ≤ 20, −29 ≤ *k* ≤ 30, , −25 ≤ *l* ≤ 24	−17 ≤ *h* ≤ 17, −32 ≤ *k* ≤ 32, −21 ≤ *l* ≤ 21	−13 ≤ *h* ≤ 13, −15 ≤ *k* ≤ 15, −16 ≤ *l* ≤ 16
reflctns utilized	37026	77824	64028	17070
indep reflctns	7569 [*R*(int) = 0.0214, R_σ = 0.019]	15968 [*R*(int) = 0.1010, R_σ = 0.097]	12312 [*R*(int) = 0.1866, R_σ = 0.238]	6254 [*R*(int) = 0.1192, R_σ = 0.141]
redundancy	4.96	4.87	5.20	2.73
reflectn with *I* > 2σ(*I*)	5827 (77.0%)	8572 (53.4%)	4824 (39.2%)	3563 (57.0%)
completeness, %	94.4	93.5	99.6	99.8
max and min. transmission	0.8429, 0.7271	0.8372, 0.6874	0.9886, 0.8561	0.9528, 0.8897
data/restraints/params	7569/3/455	15968/168/946	12312/0/785	6254/234/721
GoF on *F*^{2}	1.031	1.036	0.930	1.024
final *R* indices [*I* > 2σ(*I*)]	R_1 = 0.0535, wR$_2$ = 0.1404	R_1 = 0.0739, wR$_2$ = 0.1882	R_1 = 0.0759, wR$_2$ = 0.1558	R_1 = 0.0806, wR$_2$ = 0.1621
R indices (all data)	R_1 = 0.0725, wR$_2$ = 0.1606	R_1 = 0.1504, wR$_2$ = 0.2456	R_1 = 0.1997, wR$_2$ = 0.1895	R_1 = 0.1555, wR$_2$ = 0.1897
largest diff. peak and hole, e/Å^3	0.682 and −0.412	0.674 and −0.766	0.582 and −0.567	0.749 and −0.664
RMS diff density, e/Å^3	0.075	0.097	0.085	0.075

achieved utilizing direct (or in some cases Patterson) methods followed by Fourier synthesis. Hydrogen atoms were added at idealized positions, constrained to ride on the atom to which they are bonded, and were given thermal parameters equal to 1.2 or 1.5 times U_{iso} of that bonded atom. Empirical absorption and decay corrections were applied using the program SADABS.[46] Scattering factors and anomalous dispersion were taken from International Tables (Volume C, Tables 4.2.6.8 and 6.1.1.4.).

***paral*-[FeOMTPP(1-MeIm)₂]Cl.** A purple block of $FeN_4C_{52}H_{44}$· $2(N_2C_4H_6)$·(Cl)·(CD_2Cl_2) was crystallized from methylene chloride-d_2/dodecane. The asymmetric unit contains one porphyrin molecule, one solvent (CD_2Cl_2), and chloride as a counterion. All molecules are on the general positions. Both solvent and chloride were refined by splitting them into two pieces. The population of each part was refined to 0.85:0.15 and 0.77:0.23 for CD_2Cl_2 and chloride, respectively. Solvent disorder is due to a solvent rocking motion.

***perp*-[FeOMTPP(1-MeIm)₂]Cl.** A dark red tetrahedron of FeN_4-$C_{52}H_{44}$·$2(N_2C_4H_6)$·(Cl)·2.43($CDCl_3$) was crystallized from chloroform-d/cyclohexane. The unit cell of *perp*-[FeOMTPP(1-MeIm)₂]Cl contains 12 porphyrin molecules that occupy $\bar{4}$ positions. After completing the initial structure solution, it was found that 25% of the cell volume was filled with disordered solvent. First, solvent was modeled as discrete molecules. There were 32 chloroform molecules that occupy two different C_3 positions, and 12 chloride ions, which sit on C_3 positions. There are 16 C_3 special positions in the $I\bar{4}3d$ group, but only $^3/_4$ of them are occupied with chloride anion, giving 12 chlorides, which balances the charge of 12 porphyrins. Chloroform molecules and chlorides occupy distinct channels in the crystal; therefore they were highly disordered. Analysis of solvent voids using Platon[47] gave a volume of 4376.1 Å³/cell. From this point on, atoms in the solvent region including counterion (Cl⁻) were removed and the solvent region was refined as a diffuse contribution without specific atom positions using the Platon module SQUEEZE.[48] Four voids with volume of 1085−1086 Å³ were found in the unit cell. Each void contained 477−479 electrons, giving a total of 1913 electrons/cell. The given electron count and volume can be accounted for by 12 Cl⁻ and 29.2 $CDCl_3$ per unit cell. While not part of the atom list, these are included in the formulas, F000, density, and absorption coefficient. An improvement was observed in all refinement parameters and indices except GoF which increased by 0.2.

As was already mentioned, the porphyrin molecules occupy $\bar{4}$ positions. Therefore only $^1/_4$ of the porphyrin is present in the asymmetric unit. Due to the symmetry of the molecule, the 1-methylimidazole (1-MeIm) ligands are 2-fold disordered. Each of them was modeled using two parts: one contained three nitrogens in positions 1, 3, 4 (numbering starts at the ligated nitrogen) and two methyl groups attached to nitrogens in positions 3 and 4. The second molecule had only one nitrogen in position 1 and no methyl group. Both parts of the 1-MeIm molecule were assigned half occupancy, giving on average one "normal" 1-MeIm molecule. All distances in 1-MeIm molecules were fixed with appropriate values for ordered 1-MeIm (data taken from the structure for *paral*-[FeOMTPP(1-MeIm)₂]Cl) and the coordinates and anisotropic parameters for N2 and N4 (nitrogens that are coordinated to iron) of the axial ligand were forced to be the same.

[FeOETPP(1-MeIm)₂]Cl. A dark purple block of $FeN_4C_{60}H_{60}$· $2(N_2C_4H_6)$·(Cl)·2($CDCl_3$)·(C_6H_{12}) was crystallized from chloroform-d/cyclohexane in the course of 10 days. The asymmetric unit contains one porphyrin, one chloride, a cyclohexane, and two chloroform molecules. All of them occupy general positions. Distances and angles in cyclohexane were fixed to idealize values. There is no disorder present.

[FeTC₆TPP(1-MeIm)₂]Cl. A dark blue block of $FeN_4C_{60}H_{52}$· $2(N_2C_4H_6)$·(Cl)·2(CD_2Cl_2) was crystallized from methylene chloride-d_2/dodecane. The unit cell contains 4 porphyrin molecules that occupy $\bar{4}$ positions, 8 methylene chloride molecules that sit on general positions around the $\bar{1}$ position, and 4 chloride counterions, which sit on general positions around $\bar{4}$. Due to the symmetry found in the molecule, the ligands are 2-fold disordered. They were modeled in the same way as in the case of *perp*-[FeOMTPP(1-MeIm)₂]Cl. The tetra-β,β'-tetramethylene substituents (namely, C8, C9, and C10) on β-carbons were disordered between two sites due to thermal motion. The population of each part was refined to 0.83:0.17. The methylene chloride molecule is disordered between two sites. As was already mentioned, the CD_2Cl_2 sits on a general position. In $I\bar{4}_1/a$ there are 16 general positions. However, in a given unit cell CD_2Cl_2 molecules occupy only 8 of them and in a different unit cell they occupy different 8 positions, giving on average all 16 positions occupied with 0.5 occupancy. These two sites are related by an inversion center. The chloride anion was disordered between 4 sites with each having $^1/_4$ occupancy.

A:[FeOMTPP(4-Me₂NPy)₂]Cl. A dark red irregular block of $FeN_4C_{52}H_{44}$·$2(N_2C_7H_{10})$·(Cl)·4(CD_2Cl_2) was crystallized from methylene chloride-d_2/dodecane. The porphyrin molecule as well as the chloride anion sits on the 2-fold axis, and solvent molecules (CD_2Cl_2) are on general positions. That is why the asymmetric unit contains only half of the porphyrin molecule, 2 solvent molecules, and half of the chloride anion for charge balance. Both methylene chloride molecules are disordered between two sites (relative population is 0.5) due to a rocking motion.

B:[FeOMTPP(4-Me₂NPy)₂]Cl. A dark red distorted parallelepiped of $FeN_4C_{52}H_{44}$·$2(N_2C_7H_{10})$·(Cl)·4($CDCl_3$) was crystallized from chloroform-d/cyclohexane. Many crystals were tried but all of them were nonmerohedral twins. Data were still acquired. Only the major component of the data was integrated, using GEMINI Twinning Solution Program Suite.[49] Overlaps were ignored. The asymmetric unit contains one porphyrin molecule, 4 solvent molecules, and the chloride anion. All molecules occupy general positions. Three of the $CDCl_3$ molecules form hydrogen bonds to the chloride anion. Three out of four $CDCl_3$ molecules are disordered between two sites with equal population and the same coordinates and anisotropic parameters for carbon atoms. This disorder is due to rotational motion of the $CDCl_3$ molecule. The fourth $CDCl_3$ molecule is disordered between two sites with equal population and the same coordinates and anisotropic parameters for all Cl atoms. This disorder is due to an "umbrella-in-the-wind" motion of the $CDCl_3$ molecule.

C:[FeOMTPP(2-MeHIm)₂]Cl. A dark purple plate of $FeN_4C_{52}H_{44}$· $2(N_2C_4H_6)$·(Cl)·2($CDCl_3$)·(C_6H_{12}) was crystallized from chloroform-d/cyclohexane. Empirical absorption and decay corrections were applied using the program SADABS.[46] Following parameters were obtained: $g = 0.4739$, and $T_{min}/T_{max} = 0.883598$. The g value does not seem reasonable and indicates overcorrection of the data and the T_{min}/T_{max} ratio does not agree well with the one predicted based upon crystal dimension and absorption parameters of the atoms (see Table 1); therefore uncorrected data were used for crystal refinement.

The asymmetric unit contains one porphyrin molecule, one chloride, two chloroforms, and a cyclohexane molecule. All molecules occupy general positions. One of the solvent molecules (C600) is disordered between two sites due to rotational motion around its carbon. Therefore the coordinates and anisotropic parameters of carbon atoms from the two parts were fixed to be the same. The population was refined to 0.62:0.38 (C600:C700). All other solvent molecules are relatively well ordered. There are hydrogen bonds between the chloride and N1 of the axial ligands and carbon atoms of chloroform molecules.

D:[FeOMTPP(2-MeHIm)₂]Cl. A dark blue parallelepiped of $FeN_4C_{52}H_{44}$·$2(N_2C_4H_6)$·(Cl)·3(CD_2Cl_2) was crystallized from methylene

(45) Bruker (2002) SHELXTL Reference Manual Version 6.0, Bruker AXS Inc., Madison, WI.
(46) Sheldrick, G. SADABS 2.3, 2002.
(47) Spek, A. L. *Acta Crystallogr.* **1990**, *A46*, C-34.
(48) Van der Sluis, P.; Spek, A. L. *Acta Crystallogr.* **1990**, *A46*, 194−201.
(49) Bruker (1999) GEMINI Twinning Solution Program Suite Version 1.0, Bruker AXS Inc., Madison, WI.

chloride-d_2/dodecane. The asymmetric unit contains one porphyrin molecule, three solvent (CD_2Cl_2) molecules, and chloride as a counterion. All molecules are on general positions. There is no disorder present in this crystal. There are hydrogen bonds between the chloride and the H atom attached to N1 of the axial ligands and the D atoms attached to carbon atoms of methylene chloride molecules.

Results and Discussion

[FeOMTPP(L)$_2$]Cl with 1-methylimidazole, 4-(dimethylamino)pyridine, and 2-methylimidazole were each obtained in two different crystalline forms, from methylene chloride/dodecane and chloroform/cyclohexane solvent systems. In addition, [FeO-ETPP(1-MeIm)$_2$]Cl and [FeTC$_6$TPP(1-MeIm)$_2$]Cl were each obtained in one crystalline form from chloroform-d/cyclohexane and methylene chloride-d_2/dodecane, respectively. Atomic coordinates, complete bond length and angles table, anisotropic thermal parameters, hydrogen coordinates and complete torsion angles for all complexes in this study are listed in Tables S1–S40 in the Supporting Information.

***paral*-[FeOMTPP(1-MeIm)$_2$]Cl.** The molecular structure of *paral*-[FeOMTPP(1-MeIm)$_2$]Cl together with the numbering scheme for crystallographically unique atoms is displayed in the ORTEP diagram of Figure 1. The molecule is nonplanar and adopts an almost purely saddled conformation with axial ligands in near parallel planes. This is evident from Figures 1 and 2 as well as from the linear display shown in Figure S1 of the Supporting Information. Figure 2 displays the deviation of all the atoms from the mean porphyrin plane together with the arrangement of the axial ligands. The average deviations of the pyrrole β-Cs (1.05 Å for two opposite pyrrole rings and 0.96 Å for the other pair) as well as the average deviations of the *meso*-Cs (±0.01 Å) from the 25-atom mean porphyrin plane are consistent with the pure saddled conformation of the porphyrin core.

The saddled porphyrin core together with the peripheral substituents form two mutually perpendicular pockets, one above and one below the porphyrin mean plane. They are expected to orient two axial ligands perpendicular to each other. However, the actual dihedral angle between the planes of the axial ligands in *paral*-[FeOMTPP(1-MeIm)$_2$]Cl is 19.5°, far from being perpendicular. This is the unique feature of this structure which is, to our knowledge, the only example of a strongly saddled porphyrin core with nearly parallel axial ligand arrangement. Both axial ligands are oriented above the N1–Fe–N3 vector (Figure 1) with ligand 1, L1, (having N5 and N6) being in "correct" position (in the cavity formed by the porphyrin core and peripheral substituents) and ligand 2, L2, (having N7 and N8) in nonoptimal, "wrong" orientation (almost perpendicular to the porphyrin cavity). Despite the "wrong" orientation, L2 is closer to the N1–Fe–N3 vector than is L1: the projections of the two imidazole ligand planes onto the 25-atom mean porphyrin plane makes angles of −6.9 and 12.6° to the same N1–Fe–N3 vector for L2 and L1, respectively. Molecular mechanics calculations on [CoOETPP(L)$_2$]$^+$ (where L is 1-MeIm or 1-PhIm)[50] have shown that constraining the plane of one axial ligand to be 90° to the cavity formed by the porphyrin macrocycle increased the energy of the molecule by 72–79 kJ/mol compared to the energy minimized structure; this value should be considerably smaller for analogous OMTPPML$_2$$^+$
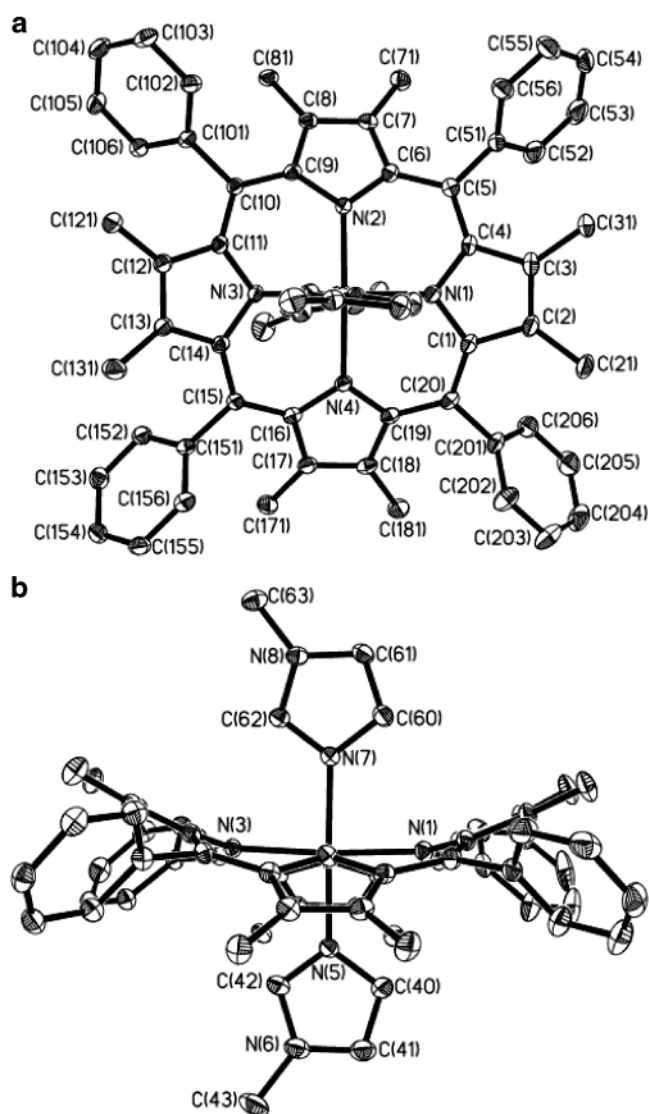
(50) Medforth, C. J.; Muzzi, C. M.; Shea, K. M.; Smith, K. M.; Abraham, R. J.; Jia, S.; Shelnutt, J. A. *J. Chem. Soc., Perkin Trans. 2* **1997**, 833–837.
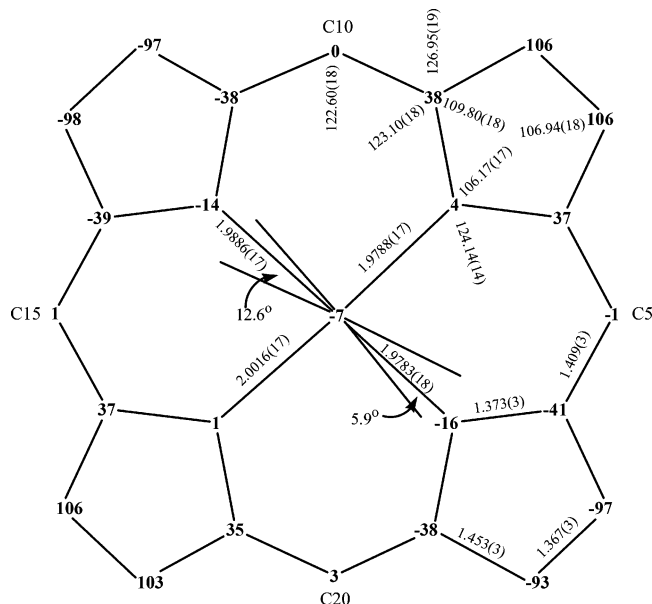
Figure 1. (a) ORTEP diagram of the porphyrin macrocycle of *paral*-[FeOMTPP(1-MeIm)$_2$]Cl with the numbering scheme for the unique atoms in the porphyrin core. Near-parallel orientation of the axial ligands can be seen clearly. (b) ORTEP plot showing numbering scheme and arrangement of axial ligands. Both methyl groups are above N3 of the porphyrin core. Thermal ellipsoids are shown at 50% probability. Hydrogen atoms have been omitted for clarity.

complexes that are not forced to have as large a saddled distortion, as shown by some DFT calculations on [FeOMTPP-(L)$_2$]$^+$ and [FeOETPP(L)$_2$]$^+$ complexes discussed below.

The question is, how, geometrically, does the purely saddled structure accommodate axial ligands in near-parallel planes? From Figure 2 one can see uneven deviations of the β-pyrrole carbons. One pair of opposite pyrrole rings deviates more from the mean porphyrin plane than does the other pair. The average deviation of the β-C is 0.96 and 1.05 Å for the first and the second pair, respectively, creating a difference of 0.09 Å. Both axial ligands are oriented along the N1–Fe–N3 axis with those two pyrrole rings (N1–C1–C2–C3–C4 and N3–C11–C12–C13–C14) having smaller deviation from planarity. In addition, N1, N3, and Fe are not in the mean porphyrin plane but slightly out of it in the direction opposite to the side having the nonoptimally oriented ligand, L2 (the deviation for the nitrogens is −0.15 Å and for Fe is −0.07 Å). On the other hand, N2 and N4 are almost in the porphyrin mean plane. These, together

Figure 2. Formal diagram of *paral*-[FeOMTPP(1-MeIm)₂]Cl showing the displacement of the atoms in units of 0.01 Å from the mean plane of the 25-atom core. The orientations of the axial ligands with the closest Fe−N$_P$ vector and selected bond angles and lengths are also shown.

with one longer Fe−N$_{ax}$ distance (2.0155(19) Å for the nonoptimally oriented ligand vs 1.9747(19) Å for the "correctly" oriented ligand) provide the room for two axial ligands along the N1−Fe−N3 vector and the "parallel" (19.5°) orientation to be possible. The axial ligands are tilted with respect to the mean porphyrin plane: the dihedral angles between each imidazole ligand and the porphyrin mean plane are 80.9 and 86.8° for L1 and L2, respectively.

As commonly found in saddled octaalkyltetraphenylporphyrins,[32] the phenyl rings rotate toward the porphyrin plane to minimize unfavorable contacts with the β substituents on the pyrrole rings. The average dihedral angles of the phenyl rings with the macrocycle plane are 45.5°, 46.0°, 50.3°, and 46.3°. This correlates with the degree of saddled distortion in the molecule: the steeper saddles result in more acute dihedral angles for the phenyl rings.[32] The average bond length between the *meso*-C and phenyl rings is 1.492(3) Å.

Other examples of Fe(III) porphyrinates with parallel imidazole ligands include [FeTMP(1-MeIm)₂]ClO₄[24] and [FeTMP-(5-MeHIm)₂]ClO₄.[20] There are two independent molecules with planar porphyrin cores and parallel ligand orientations in the asymmetric units of each structure. In the structure of [FeTMP-(1-MeIm)₂]ClO₄ the parallel imidazole planes (Δφ = 0°) form dihedral angles of 23° and 41° to the closest N$_P$−Fe−N$_P$ axis for molecules 1 and 2, respectively.[24] The imidazole planes do not lie strictly along the normal to the porphyrin core but form angles of 83.7° and 88.8° to the mean porphyrin plane.[24] In comparison, in the molecular structure of [FeTMP(5-MeHIm)₂]-ClO₄[20] the axial ligand planes are not strictly parallel; dihedral angles between the two axial ligands, Δφ, are 26° and 30° for molecules 1 and 2, respectively. The imidazole planes are tilted somewhat with respect to the mean porphyrin plane forming dihedral angles of 86.0° and 88.3° in molecule 1 and 83.2° and 86.6° in molecule 2. Near-parallel orientation of the imidazole ligands in the structures of [FeTMP(1-MeIm)₂]ClO₄[24] and [FeTMP(5-MeHIm)₂]ClO₄[20] is accompanied by nearly planar porphyrin cores. Therefore, the structure of *paral*-[FeOMTPP-

(1-MeIm)₂]Cl with a nonplanar, saddled porphyrin core and nearly parallel axial ligands is the first of its kind to be described in the literature.

The average Fe−N$_P$ distance in *paral*-[FeOMTPP(1-MeIm)₂]-Cl is 1.990(2) Å. It is slightly longer than the same distances in other porphyrins in this study (Table 2). The interesting fact is that two adjacent Fe−N$_P$ distances, Fe−N1 and Fe−N2, are similar to each other (1.9783(18) Å and 1.9788(17) Å) and shorter than the other pair (1.9886(17) Å and 2.0016(17) Å), Fe−N3 and Fe−N4, meaning that the Fe atom is not in the center of the porphyrin. Such arrangement seems to be inconsistent with the orientation of the axial ligands above and below the N1−Fe−N3 vector: we would expect Fe−N1 and Fe−N3 bonds that are almost eclipsed with the axial ligand planes, not Fe−N3 and Fe−N4 bonds, to be longer. However, similar situations, where the Fe(III) atom is not in the center of the porphyrin core, have been found for other LS Fe(III) porphyrinates.[26,51] The average Fe−N$_P$ distance in [FeTMP(1-MeIm)₂]ClO₄ of 1.995(3) Å is longer than the same distance in any of the 1-methylimidazole complexes of this study. This is due to the planarity of the porphyrin core in the TMP case. Again, it is commonly observed that a planar porphyrin core correlates with longer Fe−N$_P$ distance.[50]

***perp*-[FeOMTPP(1-MeIm)₂]Cl.** The molecular structure of *perp*-[FeOMTPP(1-MeIm)₂]Cl is displayed in Figure 3. Both the perpendicular orientation of the axial ligands and the saddled conformation of the porphyrin core are obvious. The deviation of each unique atom in the porphyrin core from the 25-atom mean plane, together with the arrangement of axial ligands and typical bond lengths and angles are shown in Figure 4. The molecule adopts a saddled conformation with some ruffling admixture. The ruffling component can be seen in the deviation of both the *meso*-Cs and the β-Cs from the porphyrin mean plane. The positions of two adjacent β-C are alternately displaced by ±0.95 and ±0.99 Å from the 25-atom mean plane, and the *meso*-Cs lie ±0.10 Å out of this plane. An unexpectedly large angle between the axial ligand plane and the closest N$_P$−Fe−N$_P$ axis (29°) is observed in this structure, as shown in Figure 4. This large angle is likely responsible for the ruffling component of the core geometry.

Because the Fe atom in the crystal of *perp*-[FeOMTPP(1-MeIm)₂]Cl occupies a $\bar{4}$ position, the asymmetric unit contains only ¼ of the porphyrin molecule, which requires 2-fold disorder of the axial ligands and an exact 90° angle between their planes. The axial ligands were modeled by splitting them into two parts and constraining only the nitrogens coordinated to Fe to have the same anisotropic parameters and coordinates (Experimental Section). After final refinement, the angle between the projection of the two parts of the axial ligand and the closest N$_P$−Fe−N$_P$ vector is 21.6° and 36.9° for the N4−C8−C9 and N2−C6−N3 parts, respectively. In other words, the measured angle between the two parts of the two imidazole ligands is 15.3°. This may mean that the barrier to axial ligand rotation is low and the ligand adopts slightly different positions in different molecules.

As was shown for saddled metalloporphyrins with five-membered aromatic axial ligands using molecular mechanics calculations with a force-field that has been applied with considerable success to the prediction of crystal structure for many highly nonplanar porphyrins,[50] axial ligand planes are

Table 2. Comparison of Structural Parameters for Complexes of This Study with Those from Related Complexes

compound	Fe–Np, Å	Fe–Nax, Å	av Δ|Cm|, Å	av Δ|Cβ|, Å	angle φ between Np–Fe–Np axis and ligand planes, deg	dihedral angle, Δφ, deg	av dihedral angles of phenyls, deg	ref
pral-[FeOMTPP(1-MeIm)$_2$]Cl·CD$_2$Cl$_2$	1.990(2)	1.975(2) 2.016(2)	±0.01	−0.96 +1.05	−12.6; 6.9	19.5	47.0	TW
perp-[FeOMTPP(1-MeIm)$_2$]Cl·2.43CDCl$_3$	1.969(7)	1.982(10)	±0.10	±0.99 ±0.95	−29.3; 60.7	90.0	46.3	TW
[FeOETPP(1-MeIm)$_2$]Cl·2CDCl$_3$·C$_6$H$_{12}$	1.970(7)	1.976(3) 1.978(3)	±0.03	±1.22 ±1.25	+9.6, +82.7	73.1	40.0	TW
[FeTC$_6$TPP(1-MeIm)$_2$]Cl·CD$_2$Cl$_2$	2.005(3)	2.005(8)	±0.26	±0.35 ±0.65	−15.3; 74.7	90.0	71.8	TW
[FeOETPP(4-Me$_2$NPy)$_2$]Cl·CDCl$_3$	1.951(5)	1.984(5) 2.099(12)	±0.28	±1.34 ±1.11	−9.0; 61.0	70.0	37.4	32
A: [FeOMTPP(4-Me$_2$NPy)$_2$]Cl·4CD$_2$Cl$_2$	1.981(2)	2.018(3) 2.021(3)	±0.42	±0.61 ±0.90	−0.8; 78.0	78.8	57.5	TW
B: [FeOMTPP(4-Me$_2$NPy)$_2$]Cl·4CDCl$_3$	1.983(3)	2.000(4) 2.003(4)	±0.07	±0.93 ±0.88	−1.0; 87.5	88.5	55.8	TW
D: [FeOMTPP(2-MeHIm)$_2$]Cl·3CD$_2$Cl$_2$	1.979(7)	2.007(7) 2.010(7)	±0.13	±0.97 ±1.08	−11.2; 69.5	80.7	49.5	TW
C: [FeOMTPP(2-MeHIm)$_2$]Cl·2CDCl$_3$	1.977(4)	2.006(5) 2.032(5)	±0.21	±0.86 ±1.04	−13.1; 71.0	82.1	53.9	TW
[FeOETPP(2-MeIm)$_2$]$^+$(SbF$_6^-$, Cl$^-$)	1.974(9)	2.09(2)	±0.09	±1.20 ±1.23	−14; 76	90	42	32
[FeTPP(2-MeHIm)$_2$]ClO$_4$	1.971(4)	2.015(4) 2.010(4)	±0.40	±0.17	−32; 57	89	76	15
[FeTMP(4-Me$_2$NPy)$_2$]ClO$_4$	1.964(10)	1.989(4) 1.978(4)	±0.51	±0.20	−37; 42	79	79	24
[FeTMP(1,2-Me$_2$Im)$_2$]ClO$_4$	1.937(12)	2.004(5) 2.004(5)	±0.72	±0.23 ±0.24	−45; 45	90	87	26
perp-[FeTMP(5-MeHIm)$_2$]ClO$_4$	1.985(6) 1.979(6) 1.988(6) 1.973(6)	1.957(6); 1.973(6)	±0.32	±0.13	−30; 46	76	82.9	20
paral-[FeTMP(5-MeHIm)$_2$]ClO$_4$	1.983(4) 1.981(5)	1.978(6); 1.961(5) 1.980(5); 1.985(5)	±0.11 ±0.05	±0.16 ±0.07	−10; 20 −14; 12	30 26	83.2 85.2	20
[FeTMP(1-MeIm)$_2$]ClO$_4$ 1 [FeTMP(1-MeIm)$_2$]ClO$_4$ 2	1.988(20) 1.987(1)	1.975(3) 1.965(3)	±0.01 ±0.08	±0.02 ±0.07	23 41	0 0	81 81	24

expected to be almost eclipsed with the closest N$_P$–Fe–N$_P$ vector (the minimum energy angle is 2−3°). However, this does not hold true in the case of *perp*-[FeOMTPP(1-MeIm)$_2$]Cl where the dihedral angle between the averaged imidazole planes and the closest N$_P$–Fe–N$_P$ vector is much larger (29.3°). Due to the symmetry found in this crystal, both ligands lie along the normal to the porphyrin mean plane (however, some off-axis positioning could be possible if it is obscured by the disorder). Both the average angle between the phenyl ring and the mean porphyrin plane and the distance from the *meso*-C to the phenyl ring are close to the corresponding values in *paral*-[FeOMTPP-(1-MeIm)$_2$]Cl (46.3° vs 47.0°; and 1.470(8) vs 1.492(3) Å for *perp*- and *paral*-[FeOMTPP(1-MeIm)$_2$]Cl, respectively).

The linear deviation of each unique atom from the mean porphyrin plane in both *paral*- and *perp*-[FeOMTPP(1-MeIm)$_2$]-Cl structures is shown in Figure S1 in the Supporting Information. It is important to note that the two complexes have extremely similar geometry of the porphyrin cores, regardless of the striking difference in the axial ligand orientations (close to parallel vs perpendicular).

[FeOETPP(1-MeIm)$_2$]Cl. The molecular structure of [FeO-ETPP(1-MeIm)$_2$]Cl together with the numbering scheme for

crystallographically unique atoms is displayed in Figure 5. The molecule is nonplanar and adopts an almost purely saddled conformation with axial ligands in near perpendicular planes. This is evident in Figures 5 and 6 as well as in the linear display shown in Figure S1 of the Supporting Information. Figure 6 displays the deviation of all the atoms from the mean porphyrin plane together with the arrangement of the axial ligands. The average deviations of the adjacent β-Cs (±1.22 Å and ±1.25 Å) as well as the average deviations of the *meso*-Cs (±0.03 Å) from the 25-atom mean porphyrin plane are consistent with the pure saddled conformation of the porphyrin core.

The actual dihedral angle between the planes of the axial ligands in [FeOETPP(1-MeIm)$_2$]Cl is 73.1°, close to the minimum angle of 70° observed thus far for iron(III) porphyrinates that have "large g_{max}" EPR spectra.[32] The projection of the two imidazole ligand planes onto the 25-atom mean porphyrin plane makes angles of 9.6° and 82.7° to the same N1–Fe–N3 vector. The nitrogens of the porphyrinate ring are not in the mean plane, but rather N1, N3 are slightly above (0.10 Å) while the other two are slightly below (−0.09 Å). The axial ligands deviate insignificantly from the normal to the mean plane of the porphyrin ring, with L1 (N5, N6) being at a dihedral
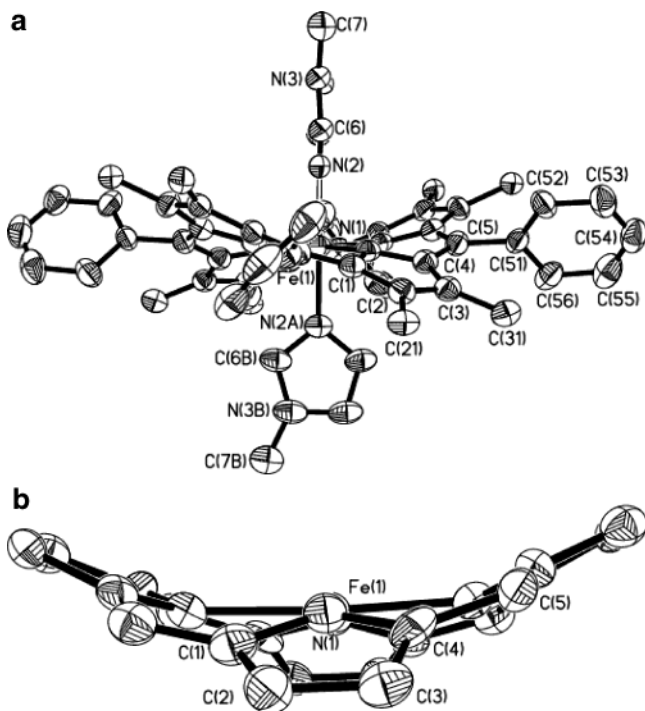
Figure 3. (a) ORTEP diagram of the porphyrin macrocycle of *perp*-[FeOMTPP(1-MeIm)$_2$]Cl with the numbering scheme for the crystallographically unique atoms. Thermal ellipsoids are shown at 30% probability. Perpendicular orientation can be clearly seen. (b) ORTEP plot showing saddled conformation of the porphyrin core. Hydrogen atoms have been omitted for clarity.
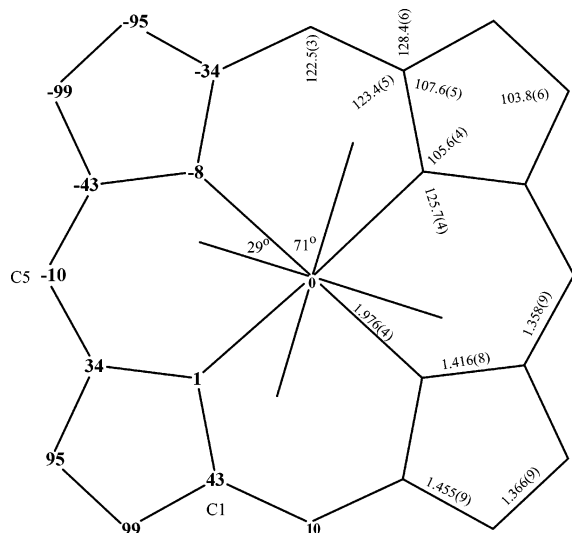

Figure 4. Formal diagram of *perp*-[FeOMTPP(1-MeIm)$_2$]Cl showing the displacement of the atoms in units 0.01 Å, from the mean plane of the 25-atom core. The orientations of the axial ligands with the closest Fe–N$_P$ vector are also drawn.

angle of 86.68° and L2 (N7, N8) having a dihedral angle of 87.51° to the porphyrin mean plane. The average Fe–N$_P$ bond length is 1.970(7) Å, very similar to that for *perp*-[FeOMTPP-(1-MeIm)$_2$]Cl and [FeOETPP(2-MeHIm)$_2$]$^+$ but longer than that for the other OETPP structure, [FeOETPP(4-Me$_2$NPy)$_2$]Cl.[32] The average Fe–N$_{ax}$ bond length is 1.977(3) Å, again similar to that of *perp*-[FeOMTPP(1-MeIm)$_2$]Cl and shorter than that of [FeOETPP(4-Me$_2$NPy)$_2$]Cl and [FeOETPP(2-MeHIm)$_2$]$^+$ [32] (Table 2).
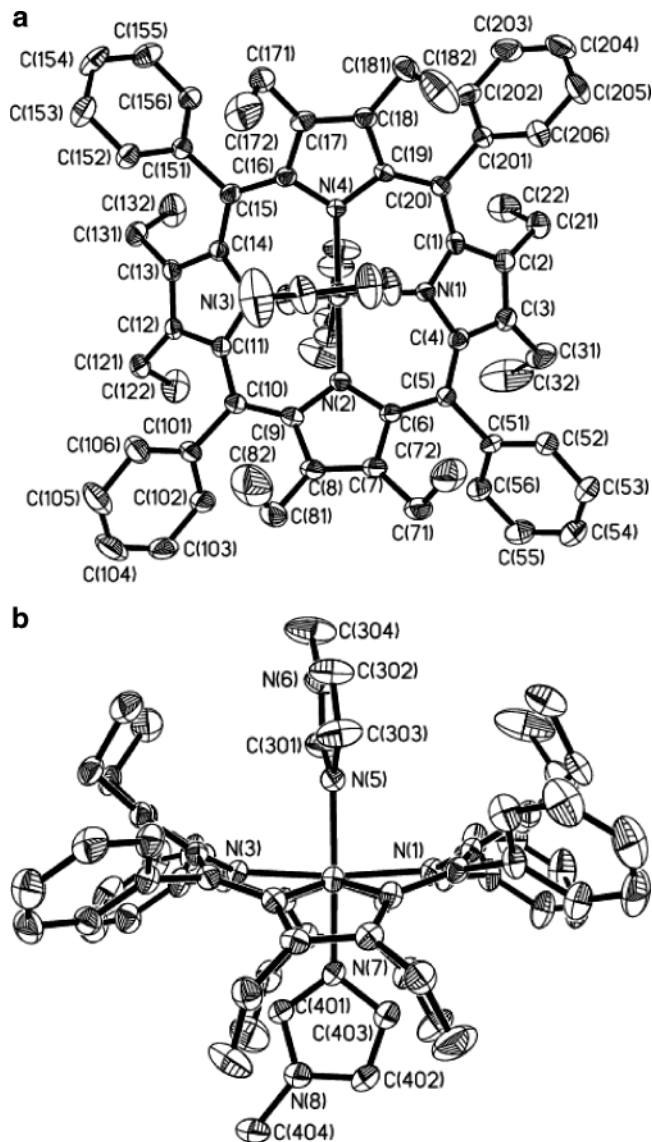

Figure 5. (a) ORTEP diagram of the porphyrin macrocycle of [FeOETPP-(1-MeIm)$_2$]Cl. Close to perpendicular orientation of the axial ligands can be clearly seen. Methyl groups of 1-methylimidazole ligands are above N2 and N3. (b) ORTEP diagram, side view, of the porphyrin core together with the numbering scheme for axial ligands. Saddled geometry is observed. Thermal ellipsoids are shown at 50% probability. Hydrogen atoms have been omitted for clarity.

The average dihedral angle of the phenyls in [FeOETPP(1-MeIm)$_2$]Cl is 40.0° (the individual values are 41.7°, 38.8°, 37.1°, and 42.3°) and is quite a bit smaller than the 46.3° and 47.0° angles observed in *perp*- and *paral*-[FeOMTPP(1-MeIm)$_2$]Cl. This is in accord with the higher saddled distortion of the former complex. The average value of the bonds between the *meso*-Cs and phenyl rings is 1.498(4) Å.

[FeTC$_6$TPP(1-MeIm)$_2$]Cl. It should first be noted that this is the only one of the [FeTC$_6$TPP(L)$_2$]Cl complexes that was crystallized. It turned out that in all other crystallization attempts the mixture did not produce any crystals but rather turned into an oil, even though two successful attempts, the (TC$_6$TPP)FeCl[53] and [FeTC$_6$TPP(1-MeIm)$_2$]Cl, produced crystals of much better quality that any other crystals of this research. The molecular structure and numbering scheme for the crystallographically unique atoms of [FeTC$_6$TPP(1-MeIm)$_2$]Cl are shown in the
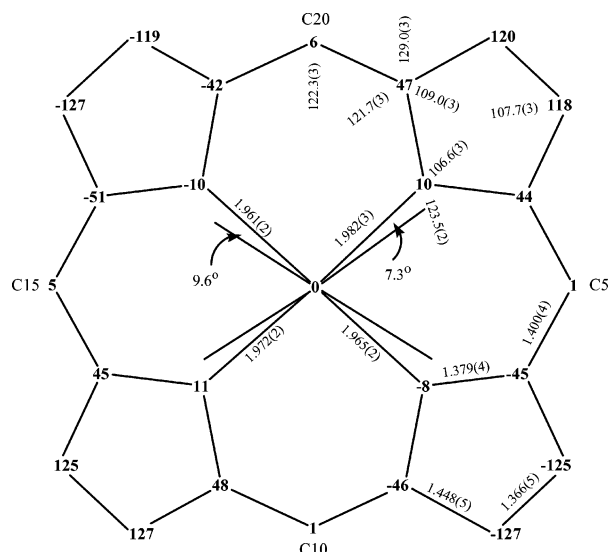
Figure 6. Formal diagram of [FeOETPP(1-MeIm)₂]Cl showing the displacement of the atoms, in units 0.01 Å, from the mean plane of the 25-atom core. The orientations of the axial ligands with the closest Fe–N_P vector are also drawn. The nearly pure saddled geometry is clearly observed.
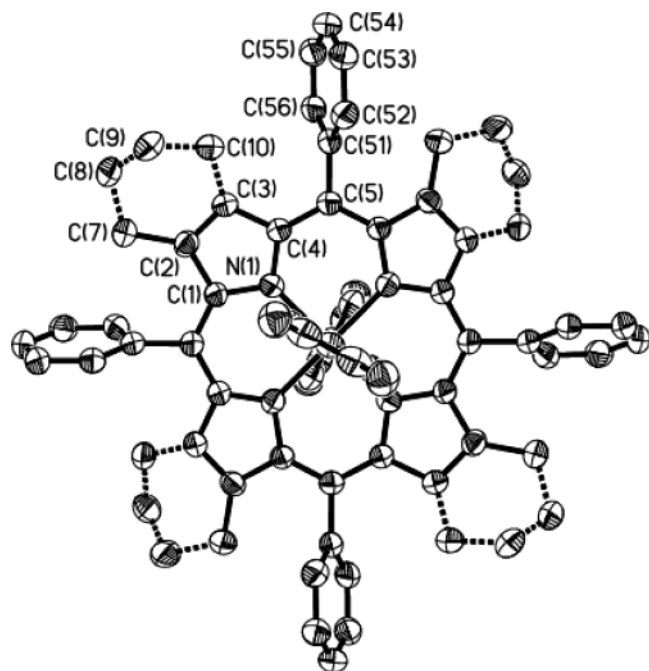

Figure 8. Formal diagram of [FeTC₆TPP(1-MeIm)₂]Cl showing the displacement of the atoms, in units 0.01 Å, from the mean plane of the 25-atom core. The orientations of the axial ligands with the closest Fe–N_P vector are also drawn. The admixture of saddled and ruffled geometry is clearly observed. Alternant pyrrole rings are still tipped above and below the porphyrin mean plane (as expected for the pure saddled conformation) but the *meso*-C are displaced above and below the porphyrin mean plane as well (as expected for the ruffled conformation).

Figure 7. ORTEP diagram of the porphyrin macrocycle of [FeTC₆TPP-(1-MeIm)₂]Cl. Thermal ellipsoids are shown at 50% probability. Perpendicular orientation of the axial ligands can be clearly seen. Hydrogen atoms have been omitted for clarity.

ORTEP diagram of Figure 7. According to the symmetry of the porphyrin molecule that sits on the $\bar{4}$ position, the planes of the axial ligands are mutually perpendicular. For the same reason they each lie along the normal to the porphyrin mean plane. Since only $^1/_4$ of the molecule is present in the asymmetric unit, the axial ligands are 2-fold disordered. They were modeled in the same way as in the case of *perp*-[FeOMTPP(1-MeIm)₂]Cl by using two different molecules with half occupancy. Both parts of the imidazole model were allowed to rotate freely and only the nitrogens coordinated to iron were constrained to have the same anisotropic parameters and coordinates. In the final model the dihedral angle between the two parts of the imidazole
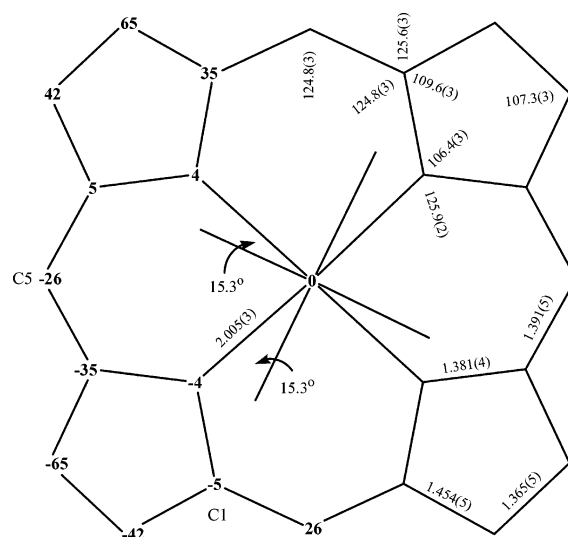
is 11.3°. Again as in the case of *perp*-[FeOMTPP(1-MeIm)₂]-Cl this may be due a slight random difference in the axial ligand arrangement throughout the crystal. The projection of the planes of the two imidazole parts on the porphyrin mean plane forms angles of 9.6 and 20.9° to the same N_P–Fe–N_P vector. Therefore the average angle is 15.3°.

The deviations of all the porphyrin atoms from the mean plane, as well as axial ligand orientations and selected bond lengths and angles are shown in the formal diagram of Figure 8. From Figure 8 and the linear diagram of the porphyrin deviation from planarity (Figure S1) one can clearly see that the porphyrin adopts an admixture of ruffled and saddled conformations. As in the purely saddled conformation, the pyrrole rings are displaced above and below the porphyrin mean plane. But as in the ruffled conformation the *meso*-Cs are no longer in the porphyrin mean plane but rather are displaced by ±0.26 Å above and below it; the pyrrole rings are twisted clockwise and counterclockwise, causing a noneven deviation for adjacent pyrrole β-Cs (±0.42 and ±0.65 Å). Using the program of Shelnutt, available on the Web[52] (Normal-Coordinate Structural Decomposition (NSD) method), the nonplanarity of the porphyrin core can be described in terms of displacements along the lowest frequency normal coordinates of the porphyrin macrocycle in order to quantify the contribution from different types of distortion (saddled, ruffled, etc.). Moreover, the sum of all the coefficients of the vibrational modes can be used to compare the degree of nonplanarity between different porphyrins: A larger sum of the vibrational coefficients correlates with a higher degree of nonplanar distortion. There are six out-of-plane displacements along the lowest frequency vibrational modes of the porphyrin macrocycle: B_{2u}(Saddle), B_{1u}(Ruffle), A_{2u}(Dome), $E_g(x)$ (Wave(x)), $E_g(y)$ (Wave(y)), and A_{1u}-(Propeller). For all the complexes of this study except *paral-*

(51) Scheidt, W. R.; Osvath, S. R.; Lee, Y. J. *J. Am. Chem. Soc.* **1987**, *109*, 1958–1963.
(52) http://jasheln.unm.edu/jasheln/content/nsd/NSDengine/.

Table 3. Normal-Coordinate Structural Decomposition (NSD)[52] of Distortion Modes of the Complexes of This Study

compound	B_{2u}, saddle	B_{1u}, ruffle	A_{2u}, dome	$E_g(x)$, wave(x)	$E_g(y)$, wave(y)	A_{1u}, propeller	sum	av $\Delta\|C_m\|$, Å	av $\Delta\|C_\beta\|$, Å	ruf/sum %
paral-[FeOMTPP(1-MeIm)$_2$]Cl·CD$_2$Cl$_2$	3.0449	0.0192	0.1793	0.0367	0.0393	0.0314	3.3508	±0.01	−0.96 +1.05	0.6
perp-[FeOMTPP(1-MeIm)$_2$]Cl·CDCl$_3$	2.9400	0.3035	0.0006	0.0000	0.0000	0.0007	3.2448	±0.10	±0.99 ±0.95	9.4
[FeOETPP(1-MeIm)$_2$]Cl·2CDCl$_3$·C$_6$H$_{12}$	3.7320	0.0792	0.0360	0.1054	0.0315	0.0108	3.9949	±0.03	±1.22 ±1.25	2.0
[FeTC$_6$TPP(1-MeIm)$_2$]Cl·CD$_2$Cl$_2$	1.6073	0.7463	0.001	0.0000	0.0000	0.0007	2.3553	±0.26	±0.35 ±0.65	31.7
A:[FeOMTPP(4-Me$_2$NPy)$_2$]Cl·CD$_2$Cl$_2$	2.3007	1.0067	0.0813	0.0000	0.0000	0.0094	3.3981	±0.42	±0.61 ±0.90	29.6
B:[FeOMTPP(4-Me$_2$NPy)$_2$]Cl·CDCl$_3$	2.7554	0.1748	0.0019	0.0593	0.0148	0.0200	3.0262	±0.07	±0.93 ±0.88	5.8
[FeOETPP(4-Me$_2$NPy)$_2$]Cl·CDCl$_3$	3.7289	0.8024	0.0494	0.0363	0.0367	0.0027	4.6564	±0.28	±1.34 ±1.11	17.2
C:[FeOMTPP(2-MeIm)$_2$]Cl·2CDCl$_3$	2.8971	0.5964	0.0058	0.0682	0.0661	0.0010	3.6346	±0.21	±0.86 ±1.04	16.4
D:[FeOMTPP(2-MeIm)$_2$]Cl·3CD$_2$Cl$_2$	3.1513	0.3786	0.0441	0.1035	0.0697	0.0245	3.7717	±0.13	±0.97 ±1.08	10.0

[FeOMTPP(1-MeIm)$_2$]Cl only two of them are of major importance: B_{2u}(Sad) and B_{1u}(Ruf). The contributions from the other types of nonplanar distortion are either small or absent. In the case of *paral*-[FeOMTPP(1-MeIm)$_2$]Cl the major contribution to the geometry of the porphyrin core comes from B_{2u}-(Saddle) and A_{2u}(Dome) (the coefficients are 3.0449 and 0.1793, respectively, see Table 3). This might be due to the near parallel ligand orientation in this complex. As for the [FeTC$_6$TPP(1-MeIm)$_2$]Cl, the degree of saddling, B_{2u}, is equal to 1.6073 and the amount of ruffling, B_{1u}, is equal to 0.7463. The contribution from other vibration modes is negligible. From the numbers obtained the conclusion can be drawn that molecular structure of [FeTC$_6$TPP(1-MeIm)$_2$]Cl consists of saddled and ruffled components in the approximate ratio 0.68:0.32. This is one of the few examples of the dodecasubstituted metalloporphyrins having a substantial degree of ruffling distortion in overall saddled structure. The other cases are (TC$_6$TPP)FeCl (38%),[53] [FeOMTPP(4-Me$_2$NPy)$_2$]Cl (30%), [FeOETPP(4-Me$_2$NPy)$_2$]Cl (17%),[32] and [FeOMTPP(4-CNPy)$_2$]ClO$_4$ (17%).[54] Even though the contribution from the ruffled component in the molecular structure of [FeTC$_6$TPP(1-MeIm)$_2$]Cl is the largest among the complexes in this study (Table 3), the angle between the imidazole ligand planes and the nearest N$_P$−Fe−N$_P$ axis (φ = 15.3°) is not the largest. When the sum of NSD parameters for [FeTC$_6$TPP(1-MeIm)$_2$]Cl is compared to the same numbers for both the [FeOMTPP(1-MeIm)$_2$]Cl and [FeOETPP(1-MeIm)$_2$]-Cl structures, one can clearly see that the former is the most planar of the three (Table 3). The same is true for the five-coordinate Fe(III) chlorides of (TC$_6$TPP)FeCl, (OMTPP)FeCl, and (OETPP)FeCl.[53]

According to molecular mechanics calculations on [CoO-ETPP(1-MeIm)$_2$]$^+$,[50] the angle of minimum energy between the projection of the axial ligand plane and closest N$_P$−Fe−N$_P$ vector is 2−3° for the saddled and 45° for the ruffled conformation for five-membered aromatic sterically nonhindered axial ligands. In the structure of [FeTC$_6$TPP(1-MeIm)$_2$]Cl the

angle is 15.3°, which is reasonably close to that calculated (around 4° smaller) for the admixture of saddled and ruffled conformation of the porphyrin core observed.

The Fe−N$_P$ distance in [FeTC$_6$TPP(1-MeIM)$_2$]$^+$ is 2.005(3) Å, the longest among Fe−N$_P$ distances for nonplanar bis-imidazole complexes with OMTPP and OETPP porphyrin cores of this study (Table 2). For the two crystalline forms of [FeOMTPP(1-MeIm)$_2$]Cl and for [FeOETPP(1-MeIm)$_2$]Cl the average Fe−N$_P$ distances are 1.969(7), 1.990(2), and 1.970(7) Å, respectively. This is in accord with molecular mechanics calculations involving [CoOETPP(L)$_2$]$^+$ and [CoT^{t}BuP(L)$_2$]$^+$ with various axial ligands,[50] where shorter Co(III)−N$_P$ distances are normally observed for more distorted porphyrins. The average Fe−N$_{ax}$ bond is 1.984(4) Å and is similar to Fe−N$_{ax}$ distances in many other nonplanar porphyrins with the same type of axial ligands (Table 2).

[FeOMTPP(4-Me$_2$NPy)$_2$]Cl. The molecular structures of the two complexes are shown in the ORTEP diagrams for [FeOMT-PP(4-Me$_2$NPy)$_2$]Cl, molecule A (Figure 9), and molecule B (Figure S2) together with the numbering scheme for crystallographically unique atoms. Figure 10 shows the perpendicular displacement of the crystallographically unique atoms from the 25-atom mean plane (in units of 0.01 Å) and the arrangement of the axial ligands. Both porphyrin molecules are nonplanar and adopt predominantly saddled conformations with a similar degree of nonplanarity. The major difference in the core geometry of A and B is the amount of ruffling present in their molecular structures (29.6% in the case of A and 5.8% for B molecules, estimated using the coefficients of the lowest frequency vibrational modes[52] (Table 3)). The average deviations of adjacent β-C are ±0.61, ±0.90 Å for molecule A and ±0.88, ±0.93 Å for B (Table 2). One can see that the pyrrole rings in A are twisted, causing strongly uneven deviation of the adjacent β-Cs, which is characteristic of a ruffled geometry. Another indication of the presence of a ruffling component is the deviation of the *meso*-carbons from the mean plane. While in A the *meso*-C are ±0.36 Å above and below the porphyrin mean plane, B has its *meso*-C almost in the porphyrin mean plane

(53) Yatsunyk L. A., Ph.D. Dissertation. University of Arizona, 2003.
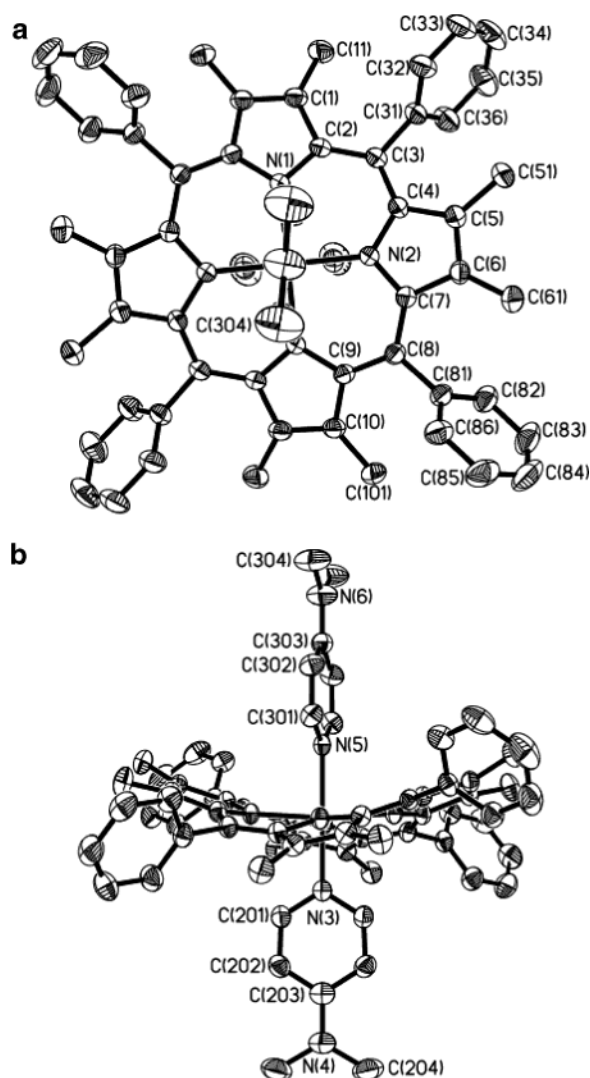(54) Yatsunyk, L. A.; Walker, F. A. *Inorg. Chem.* **2003**, *42*. In press.

a

b

Figure 9. (a) ORTEP diagram for [FeOMTPP(4-Me₂NPy)₂]Cl, molecule A. Close to perpendicular orientation of the axial ligands can be clearly seen. (b) The ORTEP diagram, showing the numbering scheme and arrangement of the axial ligands. An admixture of saddled and ruffled geometry can be seen. Thermal ellipsoids are shown at 50% probability. Hydrogen atoms have been omitted for clarity.

a

b

Figure 10. Formal diagram of the porphyrinate core in [FeOMTPP(4-Me₂NPy)₂]Cl for molecules A and B showing the displacement of the atoms, in units 0.01 Å, from the mean plane of the 25-atom core. The orientations of the axial ligands with the closest Fe–N$_P$ vector are also drawn.

(the deviation is only ±0.05 Å). Both the twisting of the pyrrole rings and the alternation in the displacements of the *meso*-Cs of the porphyrin ring are indications of significant ruffling (29.6%) in the overall saddled structure of A. A similar molecular structure is observed for [FeOETPP(4-Me₂NPy)₂]Cl reported earlier: saddled with some ruffling component.[32] The average displacements of adjacent β-Cs are ±1.13 Å and ±1.34 Å and *meso*-Cs are ±0.28 Å above and below the porphyrin mean plane (Table 2).[32] In general, the latter complex is more distorted from planarity compared to both A and B [FeOMTPP-(4-Me₂NPy)₂]Cl molecules due to the ethyl substituents on the pyrrole β positions, but it has a smaller ruffling component than A, yet larger than B.

Different geometries of the porphyrin core are observed for [FeTMP(4-Me₂NPy)₂]ClO₄ and [FeOEP(4-Me₂NPy)₂]ClO₄.[24] The [FeTMP(4-Me₂NPy)₂]ClO₄ complex is strongly ruffled with an average displacement of the *meso*-C equal to ±0.51(5) Å and the axial ligands in perpendicular planes. The same geometry of the FeTMP core is observed in the cases of other

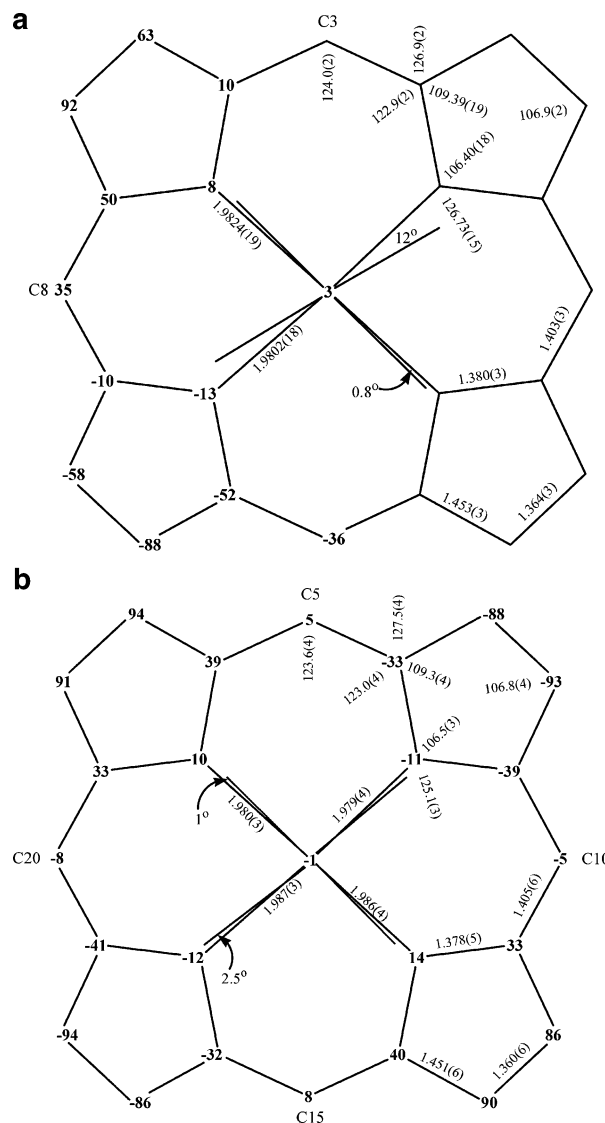bis-pyridine complexes,[25] as well as the complex with the sterically hindered 1,2-dimethylimidazole ligand.[26] In comparison, [FeOEP(4-Me₂NPy)₂]ClO₄ is essentially planar. Again, planar geometries of the FeOEP core are observed for complexes with various axial ligands and may be a property of that porphyrin core itself.[55]

The ORTEP diagrams show that the axial 4-Me₂NPy ligand planes are nearly perpendicular to each other in both structures of [FeOMTPP(4-Me₂NPy)₂]Cl (Figures 9 and S2). The actual dihedral angles between the axial ligand planes are 78.8° for molecule A and 88.5° for B. In the case of A, the dihedral angle between the axial ligands differs significantly from the expected 90° value. For the saddled [FeOETPP(4-Me₂NPy)₂]Cl complex,[32] perpendicular orientation of the axial ligands was also expected. However, the dihedral angle is 70°, the smallest among the dihedral angles observed at that time for complexes with "large g_{max}" EPR signals.[32] Significant deviation of axial ligand

(55) Geiger, D. K.; Lee, Y. J.; Scheidt, W. R. *J. Am. Chem. Soc.* **1984**, *106*, 6339–6343.

planes from the predicted perpendicular orientation is also observed in the structure of the ruffled complex [FeTMP(4-Me₂NPy)₂]ClO₄ (79°).[24] In comparison, for the case of planar [FeOEP(4-Me₂NPy)₂]ClO₄, parallel orientation of the axial ligands is observed.[24]

According to molecular mechanics calculations involving [CoOETPP(L)₂]⁺,[50] the expected angle between the projection of the six-membered aromatic axial ligands (i.e., pyridines) and the closest N_P-Fe-N_P vector of the saddled porphyrin core is 10° due to repulsion between the 2,6-H on the pyridine ligands and the nitrogens of the porphyrin. In the complexes under study, the projection of the two axial ligand planes onto the porphyrin mean plane form 0.8°, 12.0° and 1.0°, 2.5° angles to the closest N_P-Fe-N_P vector for molecules A and B, respectively. In the molecular structure of A, one of the axial ligands has close to the predicted orientation ($\varphi_1 = 12°$) and the second is essentially eclipsed with the closest N_P-Fe-N_P vector ($\varphi_2 = 0.8°$). However, the measured contact distances between the 2,6-H on the pyridine and the closest nitrogens in A are similar for both axial ligands (2.397 and 2.382 Å), as are the $Fe-N_{ax}$ bond lengths (2.018(3) and 2.021(3) Å). Even though one ligand is nearly eclipsed with the N_P-Fe-N_P axis, the geometry of the complex allows it to avoid repulsion by alternating the porphyrin nitrogen atoms above and below the porphyrin mean plane by ±0.11 Å. In the case of B both axial ligand planes are essentially eclipsed with the closest N_P-Fe-N_P vector. This still results in long enough distances between the 2,6-H of pyridine and the nitrogen atoms of the porphyrin ring (2.386, 2.355, 2.341, and 2.408 Å) to allow them to avoid steric repulsion. This is in good agreement with the molecular mechanics calculation done on [CoOETPP(Py)₂]⁺ that showed only a very small increase in the calculated energy of the complex when the structure was energy-minimized with one ligand constrained to lie exactly parallel to the $Co-N_P$ bond ($\Delta E° = 0.2$ kJ/mol).[50]

Different orientations of the axial ligands are observed in [FeOETPP(4-Me₂NPy)₂]Cl: they form 9° and 29° angles with respect to the closest N_P-Fe-N_P vector.[32] The fact that this large angle of 29° occurs despite the presence of mutually perpendicular pockets (this is true for both saddled and ruffled geometries) confirms the observation of Medforth et al.[50] that the potential energy curve for axial ligand rotation is fairly flat. The dihedral angles between the projection of axial ligand onto porphyrin mean plane and N_P-Fe-N_P vector of 37° and 42° observed in [FeTMP(4-Me₂NPy)₂]ClO₄ are typical for a predominantly ruffled geometry.[24]

The axial ligand planes in [FeOMTPP(4-Me₂NPy)₂]Cl (molecule A) and [FeOEP(4-Me₂NPy)₂]ClO₄[24] are not tilted but rather lie along the normal to the porphyrin mean plane as required by the symmetry present in the molecules (in A the porphyrin occupies the C_2 axis and in [FeOEP(4-Me₂NPy)₂]-ClO₄ the inversion center). In other structures the angles between the pyridine planes and the core show substantial deviation from perpendicular arrangement: 88.5 and 86.6°; 88.3 and 82.4°; 90 and 81.4° for [FeOMTPP(4-Me₂NPy)₂]Cl (molecule B), [FeTMP-(4-Me₂NPy)₂]⁺,[24] and [FeOETPP(4-Me₂NPy)₂]⁺,[32] respectively. These deviations from orthogonality may be due to crystal packing forces as has been suggested in previous cases.[24] However, while off-axis tilting may in some cases occur because of crystal packing forces, we find no close contacts in the

structures of the complexes that could be forcing the particular dihedral angles observed.

The angles between the planes of the phenyl rings and the mean porphyrin plane are 57.5°, 55.1°, and 57.3°, 54.4°, 54.8°, 56.6° for the A and B molecules, respectively. They are smaller compared to the same angles in [FeTMP(4-Me₂NPy)₂]⁺ (78.7° average),[24] and consistent with the predominantly saddled geometry of the present complexes. On the other hand, in planar or ruffled porphyrins the orientation of the phenyl rings is close to perpendicular with respect to the porphyrin core.

The average $Fe-N_P$ distances in A and B are very similar to each other (1.9813(19) Å and 1.983(3) Å) and to the distance in [FeOEP(4-Me₂NPy)₂]⁺ (1.986(2) Å)[24] but are much longer then the same distances in both [FeTMP(4-Me₂NPy)₂]⁺ (1.964-(10) Å)[24] and [FeOETPP(4-Me₂NPy)₂]⁺ (1.951(5) Å).[32] This agrees with the fact that both ruffled (TMP) and highly saddled (OETPP) porphyrins have shorter $Fe-N_P$ distances compared to the more planar complexes. The average $Fe-N_{ax}$ distances in [FeOMTPP(4-Me₂NPy)₂]⁺ (molecule A and B) differ substantially (2.020(3) Å and 2.002(4) Å, respectively). The same distances in all other complexes studied are shorter: 1.984(5), 2.015(6) Å; 1.989(4), 1.978(4) Å; 1.995(3) Å for [FeOETPP-(4-Me₂NPy)₂]⁺,[32] [FeTMP(4-Me₂NPy)₂]⁺,[24] and [FeOEP(4-Me₂-NPy)₂]⁺,[24] respectively.

In general, the structures of A and B have similar axial ligand orientation (the dihedral angles between the axial ligand planes are 78.8° and 88.5°, both close to perpendicular) but strikingly different porphyrin core geometries (Table 2 and Figure S1). This is opposite to what is observed in the structure of [FeOMTPP(1-MeIm)₂]Cl complexes, where the porphyrin cores have the same type of geometry but the orientation of the axial ligands is substantially different.

[FeOMTPP(2-MeHIm)₂]Cl. The molecular structures of [FeOMTPP(2-MeHIm)₂]Cl molecules C and D, together with the numbering scheme for crystallographically unique atoms are displayed in Figures S3 and 11, respectively. Figure 12 displays the value of the perpendicular displacements of the unique atoms, in units of 0.01 Å from the mean plane of the 24-atom porphyrin core for both molecules, together with the relative orientation of the axial ligands. In both cases (molecule C and D) the porphyrin molecule is nonplanar and adopts a strongly saddled conformation with a small admixture of ruffling. The average deviations of the adjacent β-carbon atoms from the mean plane are ±0.86 Å and ±1.04 Å for molecule C and ±0.97 Å and ±1.08 Å for D (Table 2). The *meso*-carbons are on average ±0.21 Å and ±0.14 Å above and below the porphyrin mean plane, for C and D, respectively. The above data, together with the parameters from NSD calculation (Table 3), indicate that both structures have saddled geometries, but molecule D is more distorted overall (the sum of all the coefficients of the vibrational modes is 3.7717, higher than that for C, 3.6346), yet has a smaller ruffling component (10% vs 16%) in comparison to molecule C. Other complexes with 2-MeHIm and other sterically hindered ligands such as 1,2-Me₂Im have been studied and reported in the literature.[15,26,32,55] All of them can be divided into three groups: those with predominantly saddled, those with predominantly ruffled nonplanar core, and those with planar porphyrin core. [FeOETPP-(2-MeHIm)₂]⁺ [32] and [FeOMTPP(2-MeHIm)₂]Cl (this work), which each have a small ruffled component in an overall saddled
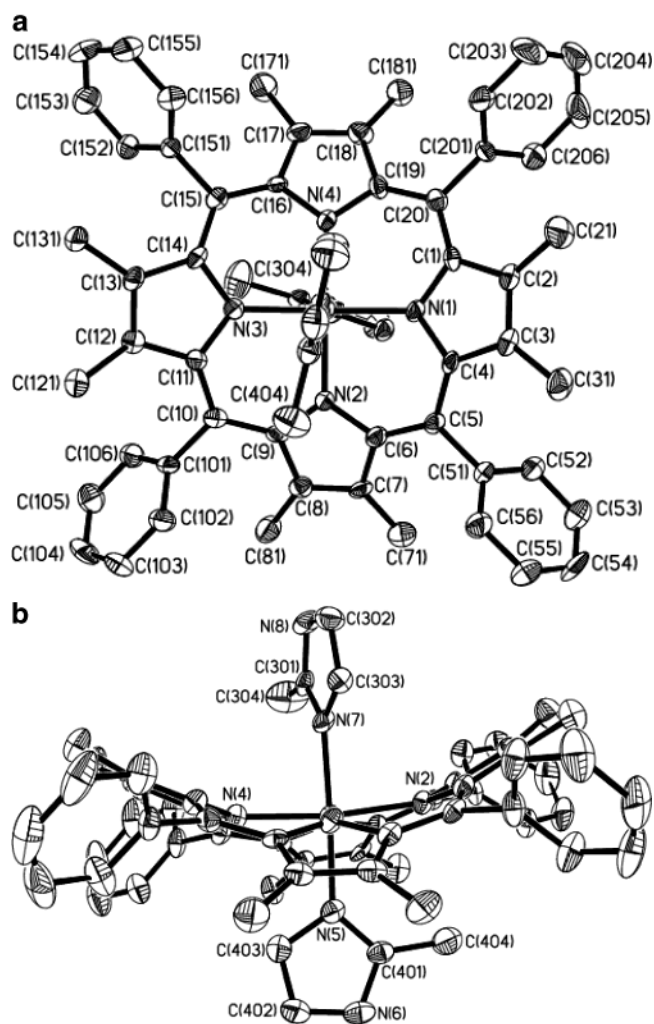
a

b

Figure 11. (a) ORTEP diagram and numbering scheme for the macrocycle of D:[FeOMTPP(2-MeHIm)₂]Cl. Methyl groups are above N2 and N3. (b) Edge-on view of the complex, showing slight distortion of the porphyrin core from pure saddled geometry. Thermal ellipsoids are shown at 50% probability. Hydrogens are omitted for clarity.

structure, belong to the first group. The former complex is more distorted from planarity overall but has a smaller degree of ruffling present.[32] The C_β of adjacent pyrrole rings in [FeO-ETPP(2-MeHIm)₂]⁺ are alternately displaced by ±1.23 Å and ±1.20 Å from the 24-atom mean plane, and the *meso*-carbons lie ±0.09 Å out of the plane. On the other hand, the porphyrin cores in the [FeTPP(2-MeHIm)₂]ClO₄[15] and [FeTMP(1,2-Me₂-Im)₂]ClO₄[26] are S_4 ruffled with the latter having the *meso*-C ±0.72 Å out of the porphyrin mean plane. This is the largest deviation observed so far in an iron(III) porphyrinate complex. And finally, the porphyrin core of [FeOEP(2-MeHIm)₂]ClO₄[55] is essentially planar. However, this complex contains high-spin Fe(III), with an Fe−N$_P$ bond length of 2.275 Å. The ~0.24−0.27 Å increase in the axial bond distance compared to other Fe(III) porphyrinates (Table 2) with hindered axial ligands is due to the change in spin state from low spin (in [FeOMTPP-(2-MeHIm)₂]Cl (this work), [FeOETPP(2-MeHIm)₂]⁺,[32] [FeTPP-(2-MeHIm)₂]ClO₄,[15] and [FeTMP(1,2-Me₂Im)₂]ClO₄[26]) to high spin in [FeOEP(2-MeHIm)₂]ClO₄.[55] Therefore, the structure of this complex is not comparable to those of the low-spin Fe(III) complexes of this study, and it will not be considered further.
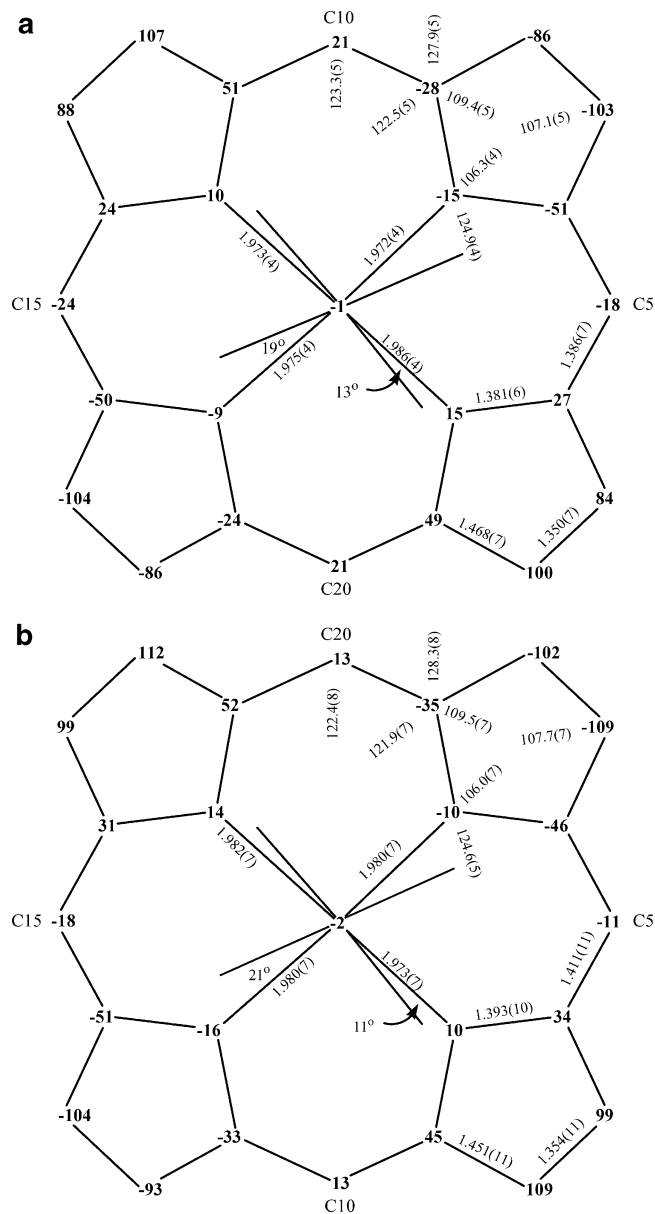
a

b

Figure 12. Formal diagrams of the porphyrinato core in [FeOMTPP(2-MeHIm)₂]Cl, C and D. All displacements are given in units of 0.01 Å. The orientations of the axial ligands with the closest Fe−N$_P$ vector and selected bond lengths and angles are also shown.

The average dihedral angles of the phenyls of 54° and 50° for C and D, respectively, are smaller compared to the same values in [FeTPP(2-MeHIm)₂]ClO₄ (76°) and [FeTMP(1,2-Me₂-Im)₂]ClO₄ (87°) and are in good agreement with the earlier finding that the phenyl dihedral angles of saddled porphyrins are all smaller than those for ruffled porphyrins.[23,35−38] When predominantly saddled complexes are compared ([FeOMTPP-(2-MeHIm)₂]⁺ (C and D) and [FeOETPP(2-MeHIm)₂]⁺[32]), the dihedral angles of the phenyls decrease in the order C (54°) > D (50°) > [FeOETPP(2-MeHIm)₂]⁺ (42°) and in the same order the degree of nonplanarity and absolute value of saddled distortion increases (judged by the B_{2u} coefficient): C (2.8971) < D (3.1513) < OETPP (3.7320). Therefore, the average value of the dihedral angles of the phenyls can be used as an indication of the degree of saddledness: the more acute dihedral angle of the phenyls correlates with the higher degree of saddled distortion.

The average Fe−N_P bond distances of 1.977(4) Å and 1.979-(7) Å for molecules C and D, respectively, are typical for other OMTPPFe(III) complexes with various axial ligands (Table 2), close to the same distance in [FeOETPP(2-MeIm)$_2$]$^+$, 1.974-(9) Å,[32] and slightly longer than the same distance in [FeTPP-(2-MeHIm)$_2$]ClO$_4$, 1.970(4) Å,[15] since the latter macrocycle is less distorted from planarity. However, the average Fe−N_P distance in [FeTMP(1,2-Me$_2$Im)$_2$]ClO$_4$, 1.937(12) Å,[26] is much shorter than the same distance in the OETPP and OMTPP saddled and TPP ruffled analogues and is the shortest reported for Fe(III) porphyrinates. This is due to the severe ruffling of the TMP porphyrin core that is usually associated with shorter Fe−N_p distances.

The bond distances, angles, and displacements from the mean porphyrin plane in [FeOMTPP(2-MeHIm)$_2$]Cl (molecules C and D) are typical for six-coordinate OMTPP complexes, as well as for other nonplanar six-coordinate porphyrin systems (OET-PP, TMP, OEP). The axial Fe−N5 and Fe−N7 bond distances are 2.006(5) and 2.032(5) Å for C and 2.007(7) and 2.010(7) Å for D. These distances are very close to those in [FeTPP(2-MeHIm)$_2$]ClO$_4$ (2.015(4) and 2.010(4) Å)[15] and in [FeTMP-(1,2-Me$_2$Im)$_2$]ClO$_4$ (2.004(5) Å)[26] but are shorter than 2.09(2) Å in [FeOETPP(2-MeHIm)$_2$]$^+$.[32]

Not all axial ligand planes lie strictly along the normal to the porphyrin mean plane. They form 81° and 85° dihedral angles with the mean porphyrin plane in [FeOMTPP(2-Me-HIm)$_2$]$^+$, molecule C, and 86° and 90° in molecule D. With this information in hand, and with the data from Figure 12, one can see that the metal in the D molecule is in a symmetrical tetragonal environment.

The orientation of the axial ligand planes in complexes with highly hindered ligands is strongly influenced by the conformation of the porphyrin macrocycle. The planes of the axial ligands in most OMTPP complexes are oriented nearly parallel to the mutually perpendicular cavities formed by the nonplanar porphyrin macrocycle and the methyl groups on the pyrrole rings. The dihedral angles between the axial ligand planes are 82.1° and 80.5° for C and D, respectively. The same angles in [FeOETPP(2-MeHIm)$_2$]$^+$,[32] [FeTPP(2-MeHIm)$_2$]ClO$_4$,[15] and [FeTMP(1,2-Me$_2$Im)$_2$]ClO$_4$[26] are 90°, 89.3°, and 89.4°, respectively.

In the case of sterically hindered axial ligands (2-MeHIm, and 1,2-Me$_2$Im) the orientation of the axial ligands is determined not only by the geometry of the pockets but also by the steric interaction between the ligands and the pyrrole N atoms. In [FeOMTPP(2-MeHIm)$_2$]Cl and [FeOETPP(2-MeHIm)$_2$]$^+$ (both mainly saddled with some ruffling) the ligands are rotated away from the N_P−Fe−N_P bond by 13.1, 19.0°; 11.2, 20.5°; and 14° for C, D, and [FeOETPP(2-MeHIm)$_2$]$^+$,[32] respectively. The observed angles can be explained mainly by steric repulsion between the methyl group of the axial ligand and the Ns of the porphyrin core and also to some extent by the presence of the ruffling component in the crystal structures of the complexes discussed. Nevertheless, the *perp*-[FeOMTPP(1-MeIm)$_2$]Cl complex has a much larger φ angle of 29° than do the 2-MeHIm complexes of either OMTPP or OETPP, supporting the suggestion that the energy profile for orientation of unhindered five-membered axial ligands is fairly flat in these saddled porphyrinates.[50] In the ruffled porphyrins the projections of the imidazole planes onto the porphyrinato core make angles of

Table 4. Hydrogen Bonds for C:[FeOMTPP(2-MeHIm)$_2$]Cl, [Å and deg]

D−H⋯A	d(D−H)	d(H⋯A)	d(D⋯A)	∠(DHA)
N(6)−H(6A)⋯Cl(1)	0.86	2.35	3.166(5)	159.3
C(500)−H(50H)⋯Cl(1)	0.98	2.55	3.459(8)	153.8
C(600)−H(60A)⋯Cl(1)	0.98	2.58	3.460(10)	149.8
C(700)−H(70A)⋯Cl(1)	0.98	2.48	3.460(10)	176.4
N(8)−H(8A)⋯Cl(1)^a	0.86	2.30	3.145(5)	169.8

^{a} Symmetry transformations used to generate equivalent atoms: $-x + 1$, $y - 1/2$, $-z + 3/2$.

Table 5. Hydrogen Bonds for D:[FeOMTPP(2-MeHIm)$_2$]Cl, [Å and deg]

D−H⋯A	d(D−H)	d(H⋯A)	d(D⋯A)	∠(DHA)
N(8)−H(8A)⋯Cl(1)	0.88	2.30	3.142(8)	160.0
N(6)−H(6A)⋯Cl(1)^a	0.88	2.21	3.093(8)	179.3
C(500)−H(50B)⋯Cl(1)	0.99	2.61	3.555(14)	158.7
C(700)−H(70B)⋯Cl(1)	0.99	2.59	3.531(12)	158.4

^{a} Symmetry transformations used to generate equivalent atoms: $x - 1$, y, z.

32° and 45° to the closest N_P−Fe−N_P vector in [FeTPP(2-MeHIm)$_2$]ClO$_4$[15] and [FeTMP(1,2-Me$_2$Im)$_2$]ClO$_4$,[26] respectively. These are expected values for ruffled iron porphyrinates.

The N6 and N8 atoms of the two 2-MeHIm ligands in each C and D structure, as well as C500, C600, and C700 of the CHCl$_3$ and C500 and C700 of CH$_2$Cl$_2$ molecules in C and D, respectively, are hydrogen bonded to Cl1 and another symmetry-generated chloride. Hydrogen bond distances and angles are presented in Tables 4 for molecule C and Table 5 for D.[32] H-bonds form an extended network through the entire crystal along the *a* axis, shown in Figures S4. In both cases the hydrogen bonds are shorter between the chloride and NH (2.30, 2.35 and 2.21, 2.30 Å, for C and D, respectively) and longer between the chloride and C−H of the solvents (2.48, 2.55, 2.58 and 2.59, 2.61 Å for C and D, respectively).

Calculation of Energy Barriers. Utilizing ab initio DFT calculations (B3LYP, 3-21G), the relative single-point energies of the porphyrin cores of FeOETPP$^+$ and two FeOMTPP$^+$ molecules were calculated to be 0.00, −61.57, and −40.84 kJ/mol. Cores were generated from the crystal structure data for [FeOETPP(4-Me$_2$NPy)$_2$]Cl[32] and two structures of [FeOMTPP-(4-Me$_2$NPy)$_2$]Cl, A and B, by substituting all the groups, Me, Et, and Ph, with Hs and removing the axial ligands. No geometry optimization was performed. It was found that the FeOMTPP$^+$ cores have lower energy than their FeOETPP$^+$ counterpart and between the two FeOMTPP$^+$ cores the one with admixture of saddled and ruffled geometry (Table 2) is stabilized by more than 20 kJ mol^{-1}. Electronic potential surfaces were calculated. The main electron density is on the porphyrin nitrogens, while the metal ion is electron deficient. Thus it reacts readily with the electron pairs of donor ligands. From the electron potential surface, the Fe atom in FeOETPP$^+$ is the least electron deficient; therefore, the addition of the pyridines gives the structure with the highest relative energy, 0.00 vs −123.45 and −118.57 kJ mol^{-1} for [FeOETPP(Py)$_2$]$^+$, [FeOMTPP(Py)$_2$]$^+$ A and B, respectively. The orientation of the pyridine ligands was taken to be the same as in the crystal structures (Table 2). Then the positions of both pyridine ligands were constrained to be 0° to the nearest N_P−Fe−N_P vector. This caused the energy of the molecules to increase by only 0.79 and 0.93 kJ mol^{-1} for [FeOMTPP(Py)$_2$]$^+$ A and B, respectively. Similar results were

obtained using molecular mechanics calculations[50] involving [CoOETPP(Py)$_2$]$^+$: the increase in the energy of the molecule, where one ligand was constrained to lie exactly parallel to the Co(III)−N$_P$ bonds was only 0.2 kJ mol^{-1} higher relative to the energy of minimized structure.[50] The increase in energy is due to the close contact between the ligand protons (H2 and H6 in the case of pyridine) and the porphyrin nitrogens.

Finally, a detailed analysis was performed on the core of B:[FeOMTPP(Py)$_2$]$^+$ in order to find the potential energy of axial ligand rotation. It was proposed from the molecular mechanics calculations for [CoOETPP(L)$_2$]$^+$ that this energy surface is fairly flat.[50] In our DFT calculations the ligands were constrained to having a dihedral angle of 88.5 ± 0.2° (the same as in the crystal structure, Table 2) and were rotated simultaneously in steps of 15°. The result of a series of calculations is shown in Figure S5. The highest energy (107.83 kJ mol^{-1}) was observed when both ligands were rotated by 90° from their crystal structure position, i.e., to positions opposing the shape of the saddled porphyrinate ring. The energy increased by 63.30 and 142.57 kJ mol^{-1} for A:[FeOMTPP(Py)$_2$]$^+$ and [FeOETPP-(Py)$_2$]$^+$, respectively, when both pyridine ligands were rotated by 90° from their original positions. It is reasonable to expect that in the case of five-membered aromatic nonhindered ligands (for example, 1-MeIm) and the OMTPP porphyrin core the increase in potential energy upon rotation of one or both of the axial ligands would be much smaller than for any OETPP case or the case of FeOMTPP$^+$ with hindered axial ligands (Py, 2-MeHIm). These small increases in energy can be readily offset by the stabilization expected from the Jahn−Teller effect for these low-spin d^5 complexes when axial ligands are not in perpendicular planes.[20] This energy offset justifies the fact that in the crystal structures reported herein so many different angles between the axial ligands are obtained and that in many cases the ligands are not in the optimized positions.

EPR Studies of Polycrystalline and Frozen Solution Samples of the Complexes of This Study. The X-band EPR spectra for the polycrystalline and solution samples of both *perp*-[FeOMTPP(1-MeIm)$_2$]Cl and *paral*-[FeOMTPP(1-MeIm)$_2$]Cl were recorded at 4.2 K and very low power settings (0.2 mW) to avoid saturation of these easily saturated signals and are shown in Figure 13. The sample with near-parallel ligand planes shows a rhombic EPR spectrum with the following *g* values: 2.71, 2.51, and 1.54; $\Sigma g^2 = 16.02$. The rhombic signal is indicative of the low spin (LS) iron(III) heme center having "parallel" ligand orientation. It was found previously[20] that even for an axial ligand plane dihedral angle as large as 30° a rhombic EPR signal is still observed. For the *paral*-[FeOMTPP(1-MeIm)$_2$]Cl complex, the small tetragonal splitting Δ/λ^{56} (1.82, compared to 2.79 for the analogous OETPP complex and especially compared to values of 3−3.5 usually observed for bis(imidazole) complexes of hemins[19]) may be a result of a longer Fe−N$_{ax}$ bond, since one ligand occupies a nonoptimal position. The rhombic splitting, V/λ, is 2.44, yielding the value of the rhombicity, V/Δ, of 1.34. The latter is twice as large as the limiting value of 0.67 for the ideal case,[56] where magnetic axes are permuted to achieve this limiting value. We have maintained the common assignment, where g_{zz} is the largest *g* value and is aligned along the normal to the average porphyrin core, as has been shown for [FeTPP(HIm)$_2$]$^+$ and a large number of related complexes.[57−59] Other similarly large values of the
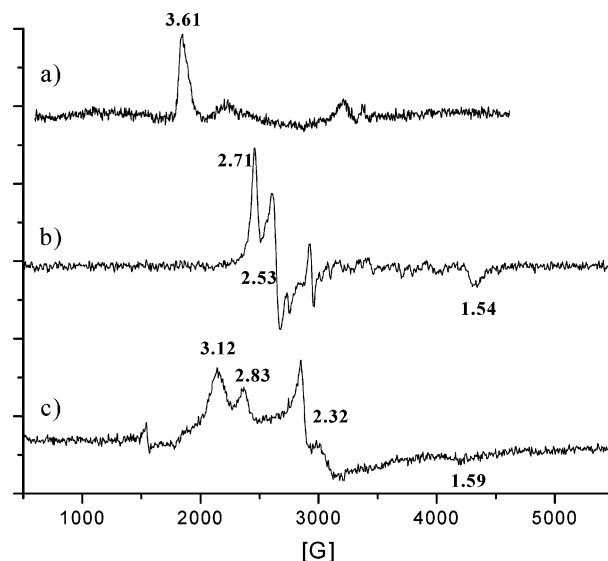
Figure 13. X-band EPR spectrum at 4.2 K for (a) *perp*-[FeOMTPP(1-MeIm)$_2$]Cl crystals grown from chloroform/cyclohexane mixture run at 0.2 mW microwave power and 1 G modulation amplitude. This spectrum is of the "large g_{max}" type with $g = 3.61$. As usual, the other two g values are not resolved. The relatively high noise level is due to the low power setting used in order to prevent saturation of the signal. (b) *paral*-[FeOMTPP(1-MeIm)$_2$]Cl crystals grown from methylene chloride/dodecane mixture. This spectrum is clearly rhombic with three g values 2.71, 2.51, and 1.54; $\Sigma g^2 = 16.02$. (c) Solution of [FeOMTPP(1-MeIm)$_2$]Cl in CD$_2$Cl$_2$. Two types of EPR signals are observed: a "large g_{max}" signal with $g = 3.12$, and a normal rhombic signal with $g = 2.84$, 2.32, and approximately 1.6.

rhombicity have been reported,[57−61] two of which involved Fe-(III) porphyrinate complexes with pyrazoles,[60,61] which are significantly weaker σ-donors than imidazoles. Hence, it is tempting to suggest that such large values of V/Δ may occur when the axial ligands are weak σ-donors *even though* the largest g value remains aligned along the heme normal.[60,61]

The rhombic splitting, $V/\lambda = 2.44$, for *paral*-[FeOMTPP(1-MeIm)$_2$]$^+$ is of the order of 700−1000 cm^{-1}, depending on the value taken for the spin−orbit coupling constant λ (300−400 cm^{-1}) for low-spin Fe(III),[19] or about 8.4−12 kJ mol^{-1}. While these values are much smaller in magnitude than the energy destabilization of axial pyridine ligands when rotated by 90° against the saddled macrocycle, found in the DFT calculations discussed above, the fact that 1-MeIm is a much less sterically demanding ligand may still suggest that these energies can offset each other.

The EPR spectrum of the polycrystalline sample of *perp*-[FeOMTPP(1-MeIm)$_2$]Cl displays a single-feature signal with $g_{max} = 3.61$. The "large g_{max}" signal is consistent with near-degeneracy of the d$_{xz}$ and d$_{yz}$ orbitals (near-axial electronic symmetry) and perpendicular orientation of the axial ligands.[24,25,62] In the polycrystalline sample of *perp*-[FeOMTPP(1-MeIm)$_2$]Cl several minor impurity signals are also present near the g values 3.0 and 2.1. Such additional signals are often observed for "large g_{max}" spectra,[7,8,14] and although they appear significant in the derivative mode spectra, they reflect only very small integrated signal areas relative to those of the large g_{max} species, and thus, there is only a small percentage of the sample with this "impurity" EPR signal. From the fits of the magnetic Mössbauer spectra reported elsewhere,[33] the values of g_{xx} and g_{yy} were estimated (0.63 and 1.53, respectively) and the crystal field parameters calculated. They show that the splitting between the
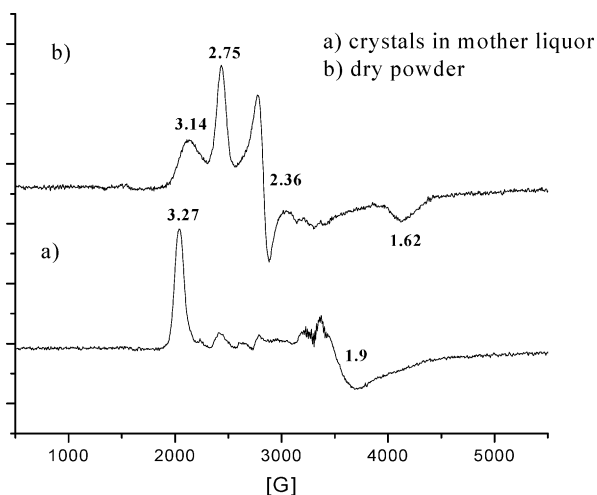
Figure 14. X-band EPR spectrum at 4.2 K of (a) [FeOETPP(1-MeIm)$_2$]-Cl crystallites immediately after isolation from the mother liquor; (b) of the same sample after 1 week at ambient temperature without the mother liquor.

d$_{xz}$ and d$_{yz}$ orbitals, *V*, is indeed small (0.67λ, where λ is the spin–orbit coupling constant).

The solution sample of [FeOMTPP(1-MeIm)$_2$]Cl in CD$_2$Cl$_2$ (Figure 13c) has rhombic (*g* = 2.83, 2.32, and ~1.59, Σg^2 = 15.92) and "large *g*$_{max}$" (*g* ~ 3.12) signals present in the EPR spectrum, as observed previously for the solution sample of [FeOETPP(1-MeIm)$_2$]Cl.[32] In the case of the rhombic signal the tetragonal splitting, Δ/λ, is 3.10 and the rhombic splitting, *V*/λ, is 2.18, yielding the value of the rhombicity, *V*/Δ, of 0.70, which is close to the ideal value of 0.67.[56] The EPR *g* values are not the same as for the polycrystalline samples, probably because the angles in the crystal are not the same as the average angles in solution. Apparently, in the solution, both parallel and perpendicular orientations of the axial ligands are possible, which is reflected in the presence of both signals in the EPR spectrum. "Large *g*$_{max}$" signals usually appear to be weak in the derivative mode because of weak transition probabilities compared to those of rhombic low-spin Fe(III) species, because these transition probabilities are proportional to the sum of the squares of the other two *g* values.[63] These two much smaller *g* values are not resolved in the EPR spectra of "large *g*$_{max}$" EPR signals because of a combination of *g* strain and a spread in the values of these two *g* values due to sample microheterogeneity. This fact makes it difficult to quantify the relative amounts of species with parallel (rhombic EPR signal) and perpendicular ("large *g*$_{max}$" EPR signal) ligand arrangement present in the frozen solution sample of [FeOMTPP(1-MeIm)$_2$]Cl.

Crystals of [FeOETPP(1-MeIm)$_2$]Cl exhibited a clean "large *g*$_{max}$" EPR signal immediately following isolation from the mother liquor, but with two resolved *g* values (3.27, 1.90), as shown in Figure 14a. From these two, the third *g* value could

(56) Taylor, C. P. S. *Biochim. Biophys. Acta* **1977**, *491*, 137−148.
(57) Quinn, R.; Valentine, J. S.; Byrn, M. P.; Strouse, C. E. *J. Am. Chem. Soc.* **1987**, *109*, 3301.
(58) Soltis, S. M.; Strouse, C. E. *J. Am. Chem. Soc.* **1988**, *110*, 2824.
(59) Astashkin, A. V.; Raitsimring, A. M.; Walker, F. A. *J. Am. Chem. Soc.* **2001**, *123*, 1905−1913.
(60) Raitsimring, A. M.; Borbat, P.; Shokhireva, T. Kh.; Walker, F. A. *J. Phys. Chem.* **1996**, *100*, 5235−5244.
(61) Schünemann, V.; Raitsimring, A. M.; Benda, R.; Trautwein, A. X.; Shokhireva, T. Kh.; Walker, F. A. *J. Biol. Inorg. Chem.* **1999**, *4*, 708−716.
(62) Palmer G. *Biochem. Soc. Trans.* **1985**, *13*, 548−560
(63) Aasa, R.; Vänngård, *J. Magn. Reson.* **1975**, *19*, 308−315.

be calculated (1.30), assuming Σg^2 = 16.[56] These values lead to calculated crystal field parameters of *V*/λ = 1.22, Δ/λ = 5.09, *V*/Δ = 0.24. However, fits of the magnetic Mössbauer spectra[33] led to a smaller value of *g*$_{yy}$ = 2.00, yielding *g*$_{xx}$ = 1.14, indicating that the second *g* value measured from the spectrum of Figure 14a probably results from a nonrandom orientation of crystallites; unfortunately the sample tube was not rotated to check this possibility. The new *g* values give *V*/λ = 1.16, Δ/λ = 3.44, *V*/Δ = 0.34; the value of the tetragonality, Δ/λ, obtained from these *g* values is much more reasonable for a complex in which the axial ligand bond lengths are equal and typical of these low-spin ferriheme complexes. It thus appears that only the largest *g* value can be reliably measured from the EPR spectra of these "large *g*$_{max}$" complexes and that the other two *g* values must be estimated from single-crystal EPR spectroscopy or the fits of magnetic Mössbauer spectra.

If the polycrystalline sample of [FeOETPP(1-MeIm)$_2$]Cl from which the EPR spectrum of Figure 14a was obtained was allowed to sit in air at room temperature for an extended period of time (allowing the loss of solvent molecules), the appearance changed from crystallites through oil to powder, and a second recording of the EPR spectrum showed that the "large *g*$_{max}$" signal had decreased in intensity and shifted to *g* = 3.14 and a new rhombic signal had appeared (*g* = 2.75, 2.36, 1.62; *V*/λ = 2.41, Δ/λ = 2.82, *V*/Δ = 0.85), Figure 14b. The EPR spectrum of the powdered material is very similar to that of the frozen solution of [FeOETPP(1-MeIm)$_2$]Cl,[32] and most probably has the same origin. It is thus due to the presence of some complex ions with axial ligand plane orientations that are close to perpendicular and others that are close to parallel. We have obtained crystals of [FeOETPP(1-MeIm)$_2$]Cl with an apparent 50° dihedral angle between the axial ligand planes that give rise to a very similar rhombic signal (*g* = 2.75, 2.34, 1.54),[53] but unfortunately there is a serious problem with this crystal structure (the crystals are probably merohedral triplets) and we have not as yet been able to solve the structure of this "parallel" form.

The EPR spectrum of the frozen solution of [FeTC$_6$TPP(1-MeIm)$_2$]Cl in CD$_2$Cl$_2$ is very similar to that of [FeOMTPP(1-MeIm)$_2$]Cl. It contains both "large *g*$_{max}$" (*g*$_{max}$ = 3.14) and rhombic (*g* = 2.86, 2.39, and 1.45; the third feature is unresolved and was calculated from the sum of *g*^{2} = 16[56]) types. From the rhombic signal *g* values, the tetragonal splitting, Δ/λ, was calculated to be 2.33 and the rhombic splitting, *V*/λ, 1.97, yields the value of the rhombicity, *V*/Δ, of 0.85, that is slightly higher than the ideal value of 0.67.[56]

The EPR spectra of frozen solutions of [FeOMTPP(4-Me$_2$-NPy)$_2$]Cl and [FeOMTPP(2-MeHIm)$_2$]Cl in CD$_2$Cl$_2$ have "large *g*$_{max}$" signals with *g* = 3.29 and 3.27, respectively. For the bis-(4-Me$_2$NPy) complex this signal is observed in the polycrystalline samples of A and B as well (*g* = 3.29). The "large *g*$_{max}$" signal is also observed for the bis(4-Me$_2$NPy) and bis(2-MeHIm) complexes of Fe(III)OETPP.[32] The difference in the "large *g*$_{max}$" *g* values of the bis(4-Me$_2$NPy) and bis(2-MeHIm) complexes of both OMTPP and OETPP is less than experimental error, while the difference between these *g* values and those of the frozen solutions of the bis(1-MeIm) complexes of OMTPP and TC$_6$TPP is considerable. Thus, it appears that while solution EPR spectra of the more sterically demanding axial ligand complexes of the octaalkyltetraphenylporphyrinato–iron(III)

systems may reflect the same *g* values as observed in the solid state, less sterically demanding axial ligand complexes produce somewhat different *g* values in frozen solution than in the solid state. This likely means that solid-state EPR data are more reliable for understanding the relationship between *g* values and molecular structure and suggests that the EPR parameters of the polycrystalline sample of *paral*-[FeTMP(5-MeHIm)$_2$]ClO$_4$ may be more characteristic of that particular structure than are the parameters obtained from the frozen solution of the complex.[20]

Conclusions. As a result of the present research, the crystal structures of five new complexes of dodecasubstituted (OMTPP, OETPP, and TC$_6$TPP) iron(III) porphyrinates with imidazole and pyridine axial ligands have been obtained. These structures provide excellent models for the cytochrome *b* heme centers. From the point of view of structural diversity, the most interesting complex is [FeOMTPP(1-MeIm)$_2$]Cl, which has been obtained in two crystalline forms with distinctly different axial ligand orientation, yet strikingly similar porphyrin core geometry. One form, *perp*-[FeOMTPP(1-MeIm)$_2$]Cl, has axial ligands in strictly perpendicular planes; the second form, *paral*-[FeOMTPP(1-MeIm)$_2$]Cl, has the particularly unusual (for a saddled porphyrinate) axial ligand dihedral angle of 19.5° and may demonstrate the energy stabilization available due to Jahn–Teller distortion of these low-spin d^5 complexes. The molecular structures of both [FeOMTPP(1-MeIm)$_2$]Cl complexes correlate nicely with the type of EPR spectra observed. Ab initio DFT calculations indicate that both perpendicular and "parallel" orientation of the axial ligands are possible.

FeOMTPP$^+$ complexes with sterically demanding axial ligands, 4-Me$_2$NPy and 2-MeHIm, have each been obtained in two crystalline forms with slightly different axial ligand orientations and porphyrin core geometries. In all four cases, the orientation of the axial ligands is very close to perpendicular and corresponds to the original expectation for these porphyrinate complexes. Quite different geometries of the porphyrin cores (from purely saddled to saddled with 30% ruffling) are observed, reflecting high flexibility of these systems. In all cases the expected "large *g*$_{max}$" signal (*g* = 3.29, 3.27), previously shown to be indicative of perpendicular ligand orientation,[7,15,24] is observed.

[FeTC$_6$TPP(1-MeIm)$_2$]Cl is the only bis-ligated complex of [FeTC$_6$TPP(L)$_2$]Cl that could be crystallized. It has a much more planar porphyrin core than in the case of either OETPP or OMTPP with 0.68:0.32 admixture of saddled and ruffled components. Axial ligands are in perpendicular orientation, as required by the symmetry of the crystal, but probably other orientations are possible as well (as is indicated by the presence of both normal rhombic and "large *g*$_{max}$" EPR signals in the frozen solution sample). On the other hand, this system is found to be too flexible for the purposes of the present research.

[FeOETPP(1-MeIm)$_2$]Cl was obtained in two crystalline forms, only one of which has, thus far, given rise to a solved crystal structure. In this case the axial ligand dihedral angle is found to be 73.1°, and the porphyrinate core is essentially purely saddled. A "large *g*$_{max}$" EPR signal (*g* = 3.27) is also observed for this complex.

In previous work we showed that a "large *g*$_{max}$" EPR signal is obtained when the dihedral angle between axial ligand planes is as small as 70°.[32] This, coupled with the finding that a normal

rhombic signal can be observed when the dihedral angle between planar axial ligands is as large as 30°[20] has narrowed the range of angles over which the type of EPR signal must switch from normal rhombic to "large *g*$_{max}$" and has modified our understanding of what "perpendicular" may actually mean in the structures of the bis-histidine-coordinated cytochromes of mitochondrial complexes II and III. However, we cannot be completely certain that the switch from normal rhombic to "large *g*$_{max}$" signal type occurs at the same axial ligand plane dihedral angle for all porphyrin ring conformations; hence it is possible that this angle may be somewhat porphyrin specific. Nevertheless, the complexes of the present study add significantly to our understanding of the flexibility of the porphyrin ring and the multiple ways in which particular axial ligand dihedral angles can be accommodated. Although we have looked carefully at the EPR data for the complexes of this study, we can find no correlation between structural features (bond lengths, axial ligand plane dihedral angles, out-of-plane distortions of porphyrin nitrogens) and the "large *g*$_{max}$" value. However, it is clear that for complexes that have a wide range of dihedral axial ligand plane angles possible the frozen solution EPR spectrum has a smaller "large *g*$_{max}$" value than that observed for the polycrystalline sample. Hence, it is as yet unclear how "large *g*$_{max}$" values as large as 3.76–3.78[6] arise for heme *b*$_L$ of mitochondrial complex III, or values of 3.41–3.44[6] arise from heme *b*$_H$, when the current structural model for that heme has the imidazole plane dihedral angle of 38°,[2,12] and model heme complexes having sugh *g*-values[7,24] have axial ligand dihedral angles of 89°[15] amd 79°.[24]

It should be emphasized that although we have utilized saddled Fe(III) porphyrinates for the present attempts to model the bis-histidine-ligated cytochromes, we are not proposing that the membrane-bound proteins have highly saddled hemes. Rather, we have used these Fe(III) octaalkyltetraphenylporphyrinates because they allow the possibility, in model heme complexes that are unconstrained with respect to their surroundings (in contrast to the heme centers in membrane-bound proteins), for axial ligands to be trapped lying close to the N$_P$–Fe–N$_P$ axes in perpendicular planes, which may stabilize Fe(II) complexes with this axial ligand arrangement. It remains to be found whether this will in fact be the case; attempts to prepare samples of the Fe(II) analogues of several of the Fe(III) complexes of the present study are underway. In the present work, we have found that Fe(III) octaalkyltetraphenylporphyrinatoiron(III) complexes provide a rich variety of axial ligand orientations and porphyrin core conformations, among which are several that lead to important insights into the possibilities for axial ligand orientations in the membrane-bound heme proteins. In fact, it can certainly be said that we have learned something important from each of the 8 structures of this study.

first EPR study of the ferrihemes of the bc_1 complex, including assignment of the spectral features observed to the three heme centers present, in 1971 (ref 5), on the occasion of his 90th birthday.

Supporting Information Available: Table S1−S5, atomic coordinates and equivalent isotropic displacement parameters; bond lengths and angles; anisotropic displacement parameters; hydrogen coordinates and isotropic displacement parameters; torsion angles for *paral*-[FeOMTPP(1-MeIm)$_2$]Cl. Tables S6−S10, S11−S15, S16−S20, S21−S25, S26−S30, S31−S35, and S36−S40: the same for *perp*-[FeOMTPP(1-MeIm)$_2$]Cl, [FeTC$_6$-TPP(1-MeIm)$_2$]Cl, A:[FeOMTPP(4-Me$_2$NPy)$_2$]Cl, B:[FeOMTPP-

(4-Me$_2$NPy)$_2$]Cl, C:[FeOMTPP(2-MeHIm)$_2$]Cl, and D:[FeOMT-PP(2-MeHIm)$_2$]Cl, and [FeOETPP(1-MeIm)$_2$]Cl, respectively. Figure S1: linear deviation of each unique atom from the porphyrin mean plane for all the structures in this study. Figures S2 and S3: ORTEP diagram for B:[FeOMTPP(4-Me$_2$NPy)$_2$]-Cl and C:[FeOMTPP(2-MeHIm)$_2$]Cl, respectively; Figure S4: hydrogen bonding network for C:[FeOMTPP(2-MeHIm)$_2$]Cl and D:[FeOMTPP(2-MeHIm)$_2$]Cl. Figure S5: calculated energy of the structure of the [FeOMTPP(Py)$_2$]$^+$ depending upon the orientation of the ligands. This material is available free of charge via the Internet at http://pubs.acs.org.

JA036398R